Shape control of lipid bilayer membranes by confined actin bundles

Feng-Ching Tsai[1] and Gijsje Hendrika Koenderink[*]

FOM Institute AMOLF, Systems Biophysics Department, Science Park 104, 1098 XG Amsterdam, The Netherlands

[*]Correspondence: gkoenderink@amolf.nl, phone +31 (0)20 754 7100

[1]Current address: Institut Curie, Laboratory PhysicoChimie Curie, 75248 Paris, Cedex 05, France

Abstract

In living cells, lipid membranes and biopolymers determine each other's conformation in a delicate force balance. Cellular polymers such as actin filaments are strongly confined by the plasma membrane in cell protrusions such as lamellipodia and filopodia. Conversely, protrusion formation is facilitated by actin-driven membrane deformation and these protrusions are maintained by dense actin networks or bundles of actin filaments. Here we investigate the mechanical interplay between actin bundles and lipid bilayer membranes by reconstituting a minimal model system based on cell-sized liposomes with encapsulated actin filaments bundled by fascin. To address the competition between the deformability of the membrane versus the enclosed actin bundles, we tune the bundle stiffness (through the fascin-to-actin molar ratio) and the membrane rigidity (through protein decoration). Using confocal microscopy and quantitative image analysis, we show that actin bundles deform the liposomes into a rich set of morphologies. For liposomes having a small membrane bending rigidity, the actin bundles tend to generate finger-like membrane protrusions that resemble cellular filopodia. Stiffer bundles formed at high crosslink density stay straight in the liposome body, whereas softer bundles formed at low crosslink density are bent and kinked. When the membrane has a large bending rigidity, membrane protrusions are suppressed. In this case, membrane enclosure forces the actin bundles to organize into cortical rings, to minimize the energy cost associated with filament bending. Our results highlight the importance of taking into account mechanical interactions between the actin cytoskeleton and the membrane to understand cell shape control.

Introduction

Cellular biopolymers are often confined by lipid membrane boundaries, which have an important impact on their overall configuration. Cytoskeletal protein filaments in animal cells such as microtubules and actin stress fibers can span across the entire cell length, which is typically on the scale of 5-100 μm. Spatial confinement offered by external constrains thus strongly affects the spatial organization of microtubules and actin stress fibers, influencing mitotic spindle positioning, cellular contractility and cell polarity [1, 2]. Cytoskeletal polymers are even more strongly confined in protrusions of the plasma membrane such as lamellipodia, filopodia, and pseudopodia. Lamellipodia are thin sheet-like protrusions (0.1 - 0.2 μm in height) filled with branched arrays of actin filaments that drive membrane protrusion in migrating cells [3-5]. Filopodia are thin cylindrical protrusions (0.1 – 0.3 μm in width) filled with parallel bundles of actin that facilitate directional cell migration, pathogen sensing, and cell-cell adhesion [4, 6]. Pseudopodia are also thin protrusions that also contribute to cell motility, but they are filled with microtubules [7, 8]. Experiments on reconstituted model systems composed of a small set of purified components have demonstrated that spatial confinement affects the conformation of actin filaments and microtubules as well as their alignment. For instance, micron-sized chambers promote spontaneous alignment of actin filaments [9, 10] and microtubules [11, 12], and thin channels straighten actin filaments by confining their thermal fluctuations [13].

Lipid membranes are fluid-like and deformable. Membrane shape remodeling can thus be achieved by interactions with membrane-associated proteins [14, 15]. Cytoskeletal polymers can also cause membrane deformation. Actin filaments for instance play an active role in forming lamellipodia and filopodia by polymerizing with their fast-growing plus ends against the plasma membrane [16]. In a similar manner, microtubules generate thin membrane protrusions such as sensory cilia [17] and axopodia [18]. Similar membrane protrusions can be formed by hemoglobin, a protein that self-assembles into semiflexible fibers in red blood cells of sickle cell disease patients [19]. Biopolymers can also influence the overall shape of cells. Marginal microtubule bands for instance contribute to the oblate shape of red blood cells [20, 21], and sickle hemoglobin fibers rigidify and deform sickle red blood cells [22, 23]. Conversely, cells can alter the mechanical properties of the plasma membrane to control cytoskeleton dynamics and organization [24-27]. In motile keratocytes, actin polymerization is suppressed at the cell rear due to the higher membrane tension, whereas the lower membrane tension at the cell leading edge allows actin polymerization [28]. Membrane tension is also a regulator of cytoskeleton architecture. It was shown that branched actin networks growing against a liposome membrane can assemble into actin bundles, deforming the membrane into protrusions, when the membrane tension is above a certain threshold [29]. Taken together, lipid membranes and biopolymers determine each other's conformation in a delicate force balance.

Motivated by the biological relevance of biopolymer confinement by membrane boundaries, there has been extensive theoretical work studying the balance of forces that governs polymer-membrane interactions [30-40]. These models generally assume an idealized case of a single polymer confined in a spherical cavity delimited either by a rigid wall or by a fluid bilayer membrane. A linear or ring-like polymer confined in a non-deformable sphere is expected to buckle and spontaneously localize underneath the spherical wall when the polymer is sufficiently stiff and the length of the polymer (ring) exceeds the confinement diameter [36]. This arrangement minimizes the enthalpic energy cost associated with polymer bending. This prediction has been experimentally confirmed by observations of microtubules confined in box-like chambers or spherical droplets, showing peripheral coil- or ring-like microtubule conformations [11, 41]. When a polymer is confined in a deformable cavity, there is a trade-off between the energy cost of bending the polymer versus the energy

cost for deforming the cavity [30, 34]. Upon increasing the rigidity of the polymer, a transition from a disordered conformation to an ordered coil is expected and the cavity will adopt an oblate shape [34]. When the polymer is infinitely stiff, depending on the polymer length or the forces exerted by the polymer on the cavity surface, various deformed cavity shapes are predicted [37, 38]. These theoretical predictions are supported by *in vitro* experiments using microtubules enclosed in liposomes. In liposomes with a high membrane tension, the membrane remains spherical and the microtubules are forced to adopt a ring-like conformation, whereas in liposomes with a low membrane tension, the microtubules remain straight and deform the membrane into finger-like protrusions [42].

Biopolymers in cells are generally not present as a single polymer, but are instead organized in dense networks or bundles. To ensure adaptability of both cytoskeletal organization and membrane shape, cells rely on a multitude of accessory proteins that crosslink the cytoskeletal filaments to each other and to the plasma membrane [43, 44]. Actin filaments are for instance organized in bundles in filopodia [6], whereas microtubules are organized in bundles in ciliae [17] and axopodia [18]. Given that bundles of biopolymers have a higher stiffness than the constituent filaments, one expects that bundling should allow for longer protrusions [45]. Experimentally, this hypothesis has been tested in a number of studies employing actin filaments enclosed in liposomes or emulsion droplets. When dense actin networks are confined in liposomes or droplets in the absence of crosslinkers, confinement forces them to arrange into a peripheral shell to minimize their bending energy [46, 47]. Indeed, with a persistence length of around 10 μm [48], actin filaments are too compliant relative to the membrane to cause membrane deformation. Cells can thus regulate the ability of actin filaments to form membrane protrusions by recruiting proteins that specifically bind actin filaments and crosslink them into bundles. Examples of well-studied bundling agents are fascin, α-actinin and filamin [49]. When actin is co-polymerized inside liposomes together with one of these bundling agents, the resulting actin bundles can deform the liposomes into various shapes, including protruded shapes [50, 51]. However, the ability of actin bundles to deform liposomes depends on both the crosslinker type and its concentration relative to that of actin. Indeed, both of these factors determine the stiffness of actin bundles [45]. It was for instance shown that bundles assembled by fascin or α-actinin are sufficiently stiff to generate membrane protrusions, in contrast to actin bundles assembled by filamin [51]. However, a systematic study where the essential parameters that govern membrane shape control by confined polymer bundles is still missing.

Here, we use cell-sized liposomes containing actin filaments bundled by fascin to provide an experimental model system where we can systematically investigate how bundled cytoskeletal polymers and a lipid membrane influence each other's configuration. By confocal microscopy and morphometric analysis, we show that actin-fascin bundles deform the liposomes into a rich set of morphologies including protruded shapes. By varying the fascin-to-actin molar ratio, we address the competition between membrane resistance and actin bundle stiffness. We find that softer bundles exhibit kinks and organize into a web-like bundle network in the main body of protruded liposomes, whereas stiffer bundles remain straight in the main body. Conversely, the configuration of the actin bundles is also determined by a competition between membrane resistance and bundle stiffness: in liposomes with a high bending rigidity, liposomes mainly remain spherical and confinement forces the actin bundles to organize into a cortical ring-like configuration underneath the liposome membrane. Our data show that lipid membranes and biopolymer bundles determine each other's conformation in a force balance that can be tuned by the membrane resistance and bundle rigidity.

Results

Liposome morphologies

To study how actin filaments and lipid membranes affect each other's organization, we develop an experimental model system consisting of cell-sized liposomes encapsulating purified actin filaments. As shown in Figs. 1*D* and *E*, actin filaments in the absence of actin crosslinkers form dense, isotropic networks inside the liposomes. In nearly half of the liposomes, actin fills the entire liposome interior (Figs. 1*D*, 2*A*, *red symbols*), forming homogeneous networks that look similar to networks formed in bulk solution (Fig. 1*A*). However, in ~60% of liposomes with a radius below 8 μm, the actin filaments concentrate into a thick cortical shell underneath the membrane (Figs. 1*E*, 2*A*, *black symbols*, and Fig. 2*B*). Spontaneous cortical actin shell formation has also been reported previously [46]. Confinement of the actin filaments by the membrane forces them to reside at the periphery so as to minimize their bending energy.

In the absence of crosslink proteins, all liposomes are spherical, with no obvious signs of membrane deformation. Indeed, the force applied by a single actin filament (at most ~1.5 pN) [52, 53] is known to be insufficient to deform a lipid bilayer membrane [54-56]. To form rigid actin bundles capable of membrane deformation, we co-polymerize actin with the crosslinker protein fascin, which is a key bundling protein in filopodia [57, 58]. We use fascin-to-actin molar ratios of 0.05 and 0.2, close to physiological values of 0.02-0.04 [59]. In bulk solution, actin and fascin co-assemble into an isotropic network of bundles (Fig. 1*B*,*C*) that are known to be unipolar and densely packed [60]. As shown in Fig. 3, assembly of these bundles inside liposomes causes dramatic membrane deformation. For any given liposome preparation, we observe a large diversity of liposome shapes (Fig. 1*F*,*G*). To systematically characterize the distribution of shapes, we observe a large population of liposomes (typically 50) per preparation. For liposomes filled with bundles at a fascin-to-actin molar ratio of R_F = 0.05, we find many liposomes having a lollipop shape, characterized by an ellipsoidal main body containing multiple actin bundles and one finger-like membrane protrusion at one pole (four examples in Fig. 3*A*). Occasionally we find ϕ-shaped liposomes with two narrow actin-filled protrusions at opposite poles (one example in Fig. 3*A*), or even liposomes with more than two protrusions (Fig. 4*A*). In addition, there are also non-protruded liposomes with a shape that is spherical, tube-like, pear-shaped, or irregular (Fig. 3*B*). To quantify the fraction of liposomes with protrusions, we classify a liposome as protruded when the width of its protrusion is at least three times smaller than the width of its main body (Fig. S1). Based on this criterion, we find that ~60% of the liposomes are protruded when $R_F = 0.05$ (out of a total of 104 liposomes). Most of the protruded liposomes have a single protrusion, whereas a minority (18%) has two or more protrusions.

To quantify the shape of each liposome, we analyze the circularity and solidity of its equatorial cross-section (see *Methods*). The *circularity* quantifies the deviation of a two-dimensional (2D) shape from a circle, and is defined as: $Circularity = 4\pi Area/Perimeter^2$. The *solidity* quantifies the degree of indentation of a 2D shape relative to a convex shape (Fig. S2*A*) [61], and is defined as: *Solidity = Area/Convex area*. *Area* denotes the area enclosed by the 2D contour of the liposome, *Perimeter* is the length of the contour, and *Convex area* is the area of a convex hull that encloses the contour. We find that both parameters clearly correlate with the classification of protruded versus non-protruded liposomes: protruded liposomes (*black symbols* in Fig. 3*C*) tend to have smaller values of both circularity and solidity than non-protruded liposomes (*red symbols*). The solidity of protruded liposomes is inversely correlated with the length of the membrane protrusion (Fig. S2*B*) and their circularity is usually below 0.4 (Fig. S2*C*). Together, the circularity and

solidity parameters therefore provide a convenient way to compare the spectrum of shapes adopted by liposomes with enclosed bundles under different experimental conditions.

When viewed in three dimensions (3D), we find that there is rarely a single bundle (only in 1 out of 21 liposomes) inside the main body of the protruded liposomes. Instead, we observe multiple bundles, regardless of the numbers of protrusions (Fig. 4*A*). These bundles usually form a planar ring-like assembly or a sparse web (Fig. 4*A n = 1 panel* and 3D-view in Fig. S3*A*), except in two liposomes that have bundles located in different planes (3D-view in Fig. S3*B*). In 25% (total 24 liposomes) of the protruded liposomes, actin bundles in the protrusions exhibit a hairpin-like bend at the tip of the protrusion, indicative of buckling (Fig. 5*C*). However, more often, the bundles exhibit sharp kinks underneath the membrane somewhere along the protrusion (Fig. 5*A*,*B*). Bundles in the main body of the liposomes also exhibit sharp kinks underneath the membrane. These kinks are suggestive of structural defects in the bundles [62], which may arise from side-branching of the bundles [63] or because actin filaments do not run along the entire bundle length [64]. Indeed, prior length measurements of actin filaments assembled in bulk solution demonstrated a broad distribution (5 to 35 μm, with an average length of 13±5 μm) with only few filaments long enough to span the entire length of an actin bundle [65].

Membrane protrusion formation

We observe a broad range of protrusion lengths, from 5 to 35 μm (Fig. 6*A*). A key question is what physical factors limit this length. It has been suggested that the length should be limited by the Euler buckling instability of the enclosed actin bundle as a result of the compressive load applied at its tip by the membrane [54-56]. The observation that for 25% of the protruded liposomes, bundles in the protrusions are buckled at their tip suggests that the buckling instability may indeed limit the protrusion length.

To directly test this hypothesis, we increase the bundle stiffness by raising the fascin-to-actin molar ratio R_F from 0.05 to 0.2, which should increase the critical Euler buckling force [66]. Overall, we observe a similar range of liposome morphologies as at low R_F, ranging from protruded liposomes having a lollipop or ϕ-shape to non-protruded liposomes that are spherical, tube-like, lemon-shaped or pear-shaped (Fig. S4*A*, *B*). The fraction of protruded liposomes is again around 60%. However, the fraction of protruded liposomes with more than one protrusion is higher at high R_F (35%, total 40 liposomes) than at low R_F (18%, total 62 liposomes). Moreover, a small number of liposomes has much longer protrusions than observed at low R_F, with lengths up to 60 μm (Fig. 6*A*). A striking difference between liposomes formed at high and low R_F is the morphology and arrangement of the actin bundles. Bundles formed at high R_F always remain straight at the protrusion tip (Fig. 5*F*) whereas the bundles formed at low R_F are occasionally (25% of cases) buckled at the tip (Fig. 5*C*). Moreover, protrusions formed at high R_F are generally straight (Figs. 4*B* and 5*F*, 78% of 32 liposomes) or occasionally (12%) gently curved (Figs. 4*B* and 5*E*), whereas protrusions formed at low R_F are sometimes sharply bent due to a kink in the supporting bundle (16% out of 44 liposomes; Fig. 5*B*). Altogether, these findings show that stiffer bundles formed at higher levels of fascin are capable of forming longer and straighter protrusions.

The arrangement of the bundles in the liposome main body is also significantly altered when the bundles are stiffened by raising R_F. In the majority of protruded liposomes (90% out of 28), the actin bundles are straight and aligned with the long axis of the liposome body at high R_F (Figs. 4*B* and 5*D*). Only 10% of the liposomes have ring-like or web-like network structures. This is in strong contrast to the low R_F case, where nearly all liposomes contain ring- or web-like arrangements of actin bundles in their main body. The shape of the main body is also somewhat more elongated at high R_F (Fig. 6*B*). These observations indicate that

stiffer bundles favor bundle alignment and liposome elongation, whereas softer bundles favor bundle bending to avoid membrane deformation.

Increasing the fascin level can increase the bundle stiffness either by increasing the number of filaments per bundle [67] or by enhancing the degree of coupling between filaments in the bundle [45]. To distinguish between these two scenarios, we compare the actin fluorescence intensity of bundles formed at low and high R_F. By normalizing the bundle intensity by the intensity of unbundled actin in the main body of each corresponding liposome (measured in-between bundles) and by assuming that this intensity represents the intensity of single filaments, we obtain an estimate of the filament number per bundle. We note that the actin fluorescence intensity in the main body among analyzed liposomes varies, indicating a variation in actin encapsulation efficiency as expected for liposomes formed by hydrogel-assisted swelling [68] (Fig. S5*A*). When we plot the actin fluorescence intensity of actin bundles against that of unbundled actin for each liposome, we do not observe a clear correlation between the two values (p = 0.5001), which indicates that the variation in actin content does not contribute to the estimated filament number per bundle (Fig. S5*B*). We emphasize that these numbers do not represent accurate absolute numbers, since the fluorescence intensity in the main body likely originates from both actin monomers and filaments. Assuming the background level to be representative of the fluorescence level of filamentous actin is, however, reasonable since the critical concentration for actin polymerization in bulk solution is typically of order 0.1 μM, which is much less than the actin concentration used (12 μM). We find that the bundle size estimated is independent of R_F, indicating that the enhanced rigidity of the bundles at high R_F is caused by tighter coupling of the filaments. Independent of R_F, bundles have an average size of 25 filaments in protrusions (Fig. 7*A black symbols*) and 15 filaments in the liposome main body (Fig. 7*A red symbols*). Line profiles reveal that some bundles in protrusions have an even fluorescence intensity along their length (Fig. 7*B right panel*), whereas others exhibit a stepwise change in intensity reflecting the convergence of multiple bundles that emanate from the main body into the protrusion (Fig. 7*B left panel*).

The experiments in which we vary bundle stiffness by varying R_F indicate that the formation of membrane protrusions is determined by a balance between bundle rigidity and membrane resistance. We can independently test this interpretation by adjusting the bending stiffness of the membrane. To this end, we dope the membrane with biotinylated lipids decorated with neutravidin, which should increase the membrane bending rigidity around 10-fold [69]. We refer to liposome membranes without neutravidin decoration as the reference membrane condition, and liposome membranes decorated with neutravidin as the stiff membrane condition. When encapsulating soft actin bundles (R_F=0.05), we observe a marked reduction of the percentage of protruded liposomes, from 60% for the reference membrane condition to 30% for the stiff membrane condition (Fig. S6), which is indeed consistent with a higher elastic energy cost for protrusion formation. The liposomes that are protruded have only a single protrusion (Fig. S7*A*). By using Alexa350-labeled neutravidin, we observe that neutravidin molecules cover the entire liposome surface including the entire protrusion (Fig. S8). The protrusions formed by stiff liposomes have a similar length as those formed with the reference membrane condition (Fig. 6*A*), but a smaller width (Fig. S9). Given that narrower membrane tubes are associated with a higher bending energy cost, this observation indicates that the protrusion width is mainly determined by membrane tension rather than bending stiffness [70]. We also observe a marked influence of membrane stiffening on the overall shape of the liposomes: both the non-protruded liposomes (Fig. S7*B-D*) and the main body of the protruded liposomes (Fig. 6*B* and Fig. S7*A*) have a significantly more circular equatorial shape than liposomes at the reference membrane condition.

The organization of the soft actin bundles (R_F = 0.05) inside the stiff liposomes is similar as in liposomes prepared at the reference membrane condition. Half of the protruded stiff liposomes have bundles with sharp kinks arranged in a planar ring-like structure in the main body, whereas the other half has distorted rings located in multiple planes (Fig. S7*A*). For the non-protruded stiff liposomes, we observe that actin bundles organize into ring-like structures underneath the membrane (Fig. S7*B* and Fig. 8*A*).

Confinement-induced actin bundle organization in non-protruded liposomes

In non-protruded liposomes, soft actin bundles (R_F = 0.05) form ring-like structures and often exhibit sharp kinks, similar to actin bundles in the main body of protruded liposomes. In nearly half of the cases, the bundles pack into a single cortical ring (Fig. 8*A panel i, packed cortical ring*), whereas in the other half, the bundles form multiple cortical rings and/or bundles that are not organized in a single plane (Fig. 8*A panel ii, multiple cortical rings*). The liposome radius (in the experimentally accessible range of 2 to 8 μm) and the membrane stiffness do not appear to affect the propensity to form a single, packed cortical ring versus multiple cortical rings (Fig. 8*B*). Comparable ring-like structures were previously reported for actin bundles formed with other types of cross-linking proteins, upon confinement in liposomes [50] or water-in-oil droplets [45], as well as for microtubules confined in liposomes [41]. Interestingly, we occasionally observe distorted ring-like actin bundles that assume a buckled shape (Fig. 8*C*) that is closely reminiscent of theoretical predictions for confined polymer rings [36].

Discussion

Morphological diversity

We use a model system of cell-sized liposomes filled with actin-fascin bundles to study the interplay of membrane-induced polymer confinement and polymer-induced membrane deformation. We focus on the cross-linking protein fascin since it has a key physiological function in forming and/or stabilizing cellular filopodia [71]. One important finding of this work is that actin-fascin bundles can drive the formation of one or more membrane protrusions only as long as the membrane is sufficiently soft. These findings are qualitatively consistent with earlier studies of liposomes deformed by actin bundles or microtubules (see below). However, we perform a more complete and quantitative analysis of liposome shapes across a large population of up to ~100 liposomes for each experimental condition. This analysis enables us to reveal a wide variety of liposome shapes differing in the degree of membrane deformation and in the spatial organization of the actin bundles. The morphological diversity we observe may be related to variations in actin encapsulation efficiency [68] and/or membrane elasticity and tension [69] among liposomes. We note that the actin encapsulation efficiency is on average about 50%, meaning that for an actin concentration of 24μM in the swelling solution, around 12μM is present inside liposomes [68]. We expect that the encapsulation efficiency for fascin will be comparable to that of actin, since actin and fascin have a comparable molecular weight, 42 and 55 kDa, respectively. Thus, we expect that the fascin-to-actin molar ratio will remain the same upon encapsulation. To assess whether there are any variations in membrane lamellarity, we measure the membrane fluorescence intensity of liposomes at the reference membrane condition and at the stiff membrane condition. As shown in Figure S10*A*, most of the liposomes in both conditions have comparable membrane fluorescence intensities, indicating uni-lamellarity [72]. Moreover, we find no correlation between membrane intensity and the likelihood of observing membrane protrusions (see Fig. S10*B*). The advantage of having a

wide range of morphologies for each liposome preparation is that it enables us to correlate membrane shape with bundle organization.

Formation and stabilization of actin-mediated membrane protrusions

Theoretical models of membrane protrusion formation by cytoskeletal filaments enclosed in a spherical liposome generally assume a single growing rod whose ends apply an axial load on the membrane [37-39, 73]. Depending on rod length and axial force, liposomes are predicted to adopt the shape of a tube, lemon, lollipop, or ϕ. We experimentally realize all the predicted shapes. Consistent with the theoretical predictions, we observe a much smaller number of liposomes with a ϕ–shape than with the energetically more favorable lollipop shape, reflecting the energy barrier for initiating each protrusion [74]. At the reference membrane condition, the percentage of ϕ-shaped liposomes is 9% (out of a total of 56 liposomes with either a ϕ–shape or lollipop shape) for soft bundles with $R_F = 0.05$ and 21% (out of a total of 33 liposomes) for stiff bundles at $R_F = 0.2$. A similar observation of a minority of ϕ-shaped liposomes was reported for liposomes encapsulating microtubules [41, 42, 75-79].

The energy required to generate a cylindrical membrane protrusion from a flat membrane arises from the mechanical energy associated with membrane stretching and bending [70]. For typical values of membrane bending rigidity (a few tens of pN·nm) and surface tension (0.001 – 0.1 pN/nm), maintaining a membrane tube with a radius of 10 - 200 nm requires a point force of 1 - 50 pN [80, 81]. However, to initiate a protrusion from a flat membrane, the applied force has to be ~13% higher than the equilibrium force [82-84]. Considering typical actin concentrations in cells (10 - 100 μM) [85], thermodynamic models predict that the maximum force generated by the polymerization of single actin filaments is around 9 pN [52]. Since this force is smaller than the typical force required to initiate and maintain a membrane tube, actin filaments need to form bundles [56, 54]. Indeed, our results clearly show that membrane protrusions are generated only if the actin filaments are bundled, in agreement with earlier, more qualitative, reports [50, 51, 86-90].

The protrusion lengths we observe for liposomes containing actin-fascin bundles (up to 60 μm) are larger than values reported earlier for liposomes containing actin bundles (3 - 12 μm) [51, 86, 87, 89, 90] or microtubules (5 – 14 μm) [41, 42, 75-79]. The difference may be due to differences in membrane composition and excess area or to differences in actin bundle stiffness. The maximum length of a membrane protrusion generated by an actin bundle is expected to be limited by the mechanical stability of the bundle against the compressive load imposed at its tip [54-56, 74]. Simply, the maximum load of a bundle can be estimated based on the critical Euler buckling force [66]. For a typical membrane resistive force of 10 - 50 pN associated with a thin membrane tube, single actin filaments with a persistence length $l_p \sim 10$ μm will already buckle for lengths longer than 40 – 100 nm. However, bundles have a larger effective persistence length that scales with the number of constituent filaments, N, as $N^{\alpha} l_p$, where α ranges from 1 to 2, depending on whether coupling is loose or tight [45]. Prior experimental data showed that actin-fascin bundles become more rigid with increasing fascin-to-actin molar ratio due to a concomitant increase of N as well as α [45]. In bulk solution, the maximum value of N for actin-fascin bundles is 20 [67], which is comparable to bundle sizes observed in filopodia (N = 10 – 20) [71, 91]. From our fluorescence intensity analysis, we also estimate N -values in this range for actin-fascin bundles assembled inside liposomes. Thus, the Euler buckling stability criterion suggests that bundles can support protrusions with a maximal length of 1 - 2 μm.

The experimentally observed lengths are much longer than expected based on the buckling criterion. This discrepancy can be explained in light of recent theoretical models, which predict that the tight enclosure of bundles by a membrane tube can prevent bundle

buckling, even for bundles composed of only 4 filaments [55, 92]. Our findings support these predictions, since we observe protrusions of up to 30 μm at low R_F and up to 60 μm at high R_F, consistent with measurements of filopodia lengths (0.4 – 100 μm) in cells [93-95]. The longest protrusions are often gently curved, consistent with predictions of the theoretical model that the membrane tube will bend together with the enclosed bundle and thus stabilize the protrusion [55]. Within this purely mechanical model, filopodia can grow to arbitrary lengths [55]. However, other factors such as G-actin diffusion to the growing filopodia tip and actin polymerization may limit the protrusion length [54, 56, 74, 96]. In our experimental assay, we are unable to observe the kinetics of bundle growth and thus cannot directly verify whether G-actin diffusion is limiting. It will be interesting to observe the kinetics of actin bundle growth in liposomes after triggering actin polymerization by introducing actin polymerization buffer via membrane channels [46, 50] or microinjection [97].

The protrusion length may also be influenced by the length distribution of the filaments within the bundles. Current theoretical models of actin-mediated membrane protrusions assume that the actin filaments within the bundle run along the entire length of the protrusion [54, 56, 98, 99]. In our experiments, however, the filament length distribution is broad and most filaments are shorter than the protrusion length. For enclosed bundles formed at low R_F, we observe sharp kinks that are reminiscent of kinks observed for actin bundles formed with the crosslinker α-actinin, which were induced by bending the bundles with optical tweezers [62]. The kinks are an indication of structural defects, which may arise from uneven filament packing in the bundles. In future, it will be informative to use fluorescently tagged fascin to identify the precise molecular basis of the kinks. It will furthermore be interesting to include the packing structure of actin bundles in theoretical models of filopodia formation, in order to be able to predict lengths and shapes of filopodia. There are observations of sharp kinks during retraction of filopodia [100] in neuronal cells [101] and macrophages [102], and helical buckling of actin inside filopodia of human embryonic kidney cells [64]. Also, there is evidence that the length of actin filaments in filopodia *in vivo* is species-dependent. For slow-growing filopodia in mouse melanoma cells, bundles of continuous actin filaments were observed [71]. However, fast-growing filopodia in *Dictyostelium* cells were shown to contain many short and contiguous filaments [91], and in the filopodia of the sea cucumber Thyone the number of actin filaments decreases down the length of the filopodium from ~200 near its base to ~10 near the tip [103], due to the influence of capping protein [104].

Our experimental model system can provide an assay to study the influence of physiological actin-membrane linkers in the future. Moreover, it provides an ideal platform to disentangle different mechanisms that have been proposed to contribute to filopodia formation, including the roles of IRSp53, formins and the Arp2/3 complex in filopodium initiation [105-110], the synergistic bundling activity of the Eps8/IRSp53 complex [111], and the effect of myosin X motors and capping protein on filopodia growth [112-114]. It would be interesting to introduce the Arp2/3 complex nucleation machinery in our system, building on recent advances in the *in vitro* reconstitution of actin nucleation at the inner surface of liposomes [115], to test the proposed mechanism of filopodia formation from dendritic arrays [116]. It will also be interesting to study a possible synergy of actin bundles with the BAR family proteins, which are shown to facilitate filopodia formation by inducing membrane deformation [117-119].

Confinement effects on actin bundle organization

Our results reveal a reciprocal influence of closed membranes and enclosed actin bundles on each other's organization. The organization of the actin bundles in the non-protruded liposomes and in the body of the protruded liposomes shows clear evidence of confinement

effects. In bulk solution, entropy favors a random spatial and orientational organization of the bundles. However, in the liposomes, the bundles are strongly confined, since the liposome diameter is comparable to the persistence length of single filaments [48, 120] and certainly much smaller than the persistence length of the bundles. Accordingly, actin bundles formed at low fascin concentration arrange in ring-like structures underneath the membrane, which avoids membrane deformation at the cost of filament bending. In contrast, stiffer bundles formed at high fascin concentration remain straight and align with the longest axis of the liposomes, which avoids filament bending but at the cost of membrane stretching.

Our findings are consistent with theoretical models of polymers confined in a rigid sphere. Ring polymers are predicted to be buckled into a distorted ring [36] and linear polymers are predicted to form a cortical ring [121]. Models of deformable liposomes containing a single polymer predict that a stiff polymer will remain straight and deform the liposome into a prolate shape, whereas a soft polymer will form a toroidal structure that deforms the liposome into an oblate shape [30, 34]. We could not test whether our liposomes have a prolate or oblate shape, since they are freely suspended in the buffer, hampering a precise 3D-reconstruction of their shape. Nevertheless, our observations are qualitatively in good agreement with these theoretical predictions. Interestingly, it has been shown that microtubules in activated blood platelets [122, 123] and in erythrocytes [21] also form a bent peripheral ring at the circumference, reminiscent of the cortical actin rings we observe in liposomes. Spontaneous ring formation may potentially aid in the formation of contractile actin-myosin rings involved in cell division [124, 125], in synergy with other mechanisms such as actin bundling by septins [126].

Conclusion

The actin cytoskeleton is an important determinant of cell shape in animals. We reconstitute a minimal model system of liposomes containing actin-fascin bundles to elucidate how a lipid membrane and a simplified actin cytoskeleton influence each other's organization through mechanical interactions. When the liposomes are sufficiently deformable, the bundles can deform the membrane into finger-like protrusions, reminiscent of cellular filopodia. The protrusions can reach lengths of up to 60 μm. In contrast, liposomes having a membrane with a large bending rigidity predominantly remain spherical and force the bundles to form cortical rings, an arrangement that minimizes the energy associated with membrane deformation as well as actin filament bending. Our results highlight the importance of taking into account the mechanical characteristics of the cytoskeleton and the plasma membrane besides factors such as biochemical signaling to understand cell shape control.

Materials and Methods

Chemicals and proteins

Chemicals were purchased from Sigma Aldrich (St. Louis, MO, USA) unless specified otherwise and lipids from Avanti Polar Lipids (Alabaster, AL, USA). We used 1,2-dioleoyl-sn-glycero-3-phosphocholine (DOPC), 1,2-dipalmitoyl-sn-glycero-3-phosphoethanolamine-N-[methoxy(polyethylene glycol)-2000] (PEG-PE), 1,2-dioleoyl-sn-glycero-3-phosphoethanolamine-N-(lissamine rhodamine B sulfonyl) (rhodamine-PE) and 1,2-dipalmitoyl-sn-glycero-3-phosphoethanolamine-N-(cap biotinyl) (biotin-PE). Neutravidin was purchased from Invitrogen (Breda, The Netherlands). Rabbit skeletal muscle monomeric actin (G-actin) was purchased from Cytoskeleton (Tebu Bio, Heerhugowaard, The Netherlands). AlexaFluor 488 labeled fluorescent actin was prepared in-house [127]. G-actin

was stored in G-buffer (2 mM Tris-HCl, 0.2 mM Na_2ATP, 0.2 mM $CaCl_2$, 1 mM DTT, pH 7.8) at 0°C for up to 1 week or at -80°C for long term storage. Before use, 4 mM DTT was added to reduce any oxidized sulfhydryl groups [128, 129], and actin solutions were clarified by centrifugation at 120,000 x *g* for 30 min and sonicated for 5 min to disrupt actin dimers [130]. Recombinant mouse fascin was prepared from T7 pGEX *E. coli* as described in [127], except that gel filtration was performed on a high-resolution Superdex 200 column (GE Healthcare, Munich, Germany). Fascin was stored at -80°C in 50 mM Tris-HCl pH 7.5, 150 mM KCl, 5 mM DTT, 10% (v/v) glycerol. Before use, fascin aliquots were clarified by centrifuging at 120,000 x *g* for 5 min and used within a week.

Liposome preparation

Liposomes with the *reference membrane condition* were prepared by swelling lipids dried on top of a layer of agarose (Type IX-A) [65]. Briefly, we spin-coated 300 µl of 1% (w/w) agarose solution on a coverslip, dried it at 37°C for 30 min, spin-coated 150 µl of a 3.75 mg/ml lipid mixture (DOPC; 0.2 mol% rhodamine-PE; 5 mol% PEG-PE) in chloroform/methanol (95:5 v/v), and dried it in vacuum for 60 min at room temperature. Liposomes decorated with neutravidin (the *stiff membrane* condition) were prepared by swelling inverse phase precursor micelles formed by adding a neutravidin solution (either 3.5 µl of 48 mg/ml or 17 µl of 10 mg/ml) to 60 µl of a 3.75 mg/ml lipid mixture (DOPC; 0.2 mol% rhodamine-PE; 2 mol% biotin-PE; 2.5 mol% PEG-PE), and pipetting up and down until the mixture became opalescent [131]. Liposomes encapsulating actin without fascin were also prepared with the precursor method, using a phosphate buffer solution to create precursors (DOPC; 0.2 mol% rhodamine-PE; 5 mol% PEG-PE). The precursor solutions (40 µl) were spin-coated on agarose-coated slides, which were then dried in vacuum for 100 min at room temperature. An open-top liposome formation chamber was assembled by placing a spacer on the agarose-lipid coated coverslip. Lipid swelling was initiated by pipetting 50 µl of an inner buffer (I-buffer: 25 mM imidazole-HCl pH 7.4, 50 mM KCl, 2 mM $MgCl_2$, 1 mM DTT, 0.1 mM $MgATP_2$, 280 mM sucrose, 2 mM trolox, 2.5 mM protocatechuic acid and 0.1 µM protocatechuate 3,4-dioxygenase) into the formation chamber. The actin concentration in the I-buffer was 23.8 µM (1 mg/ml, including 20 - 30 mol% of AlexaFluor 488 labelled actin), leading to an average actin concentration after encapsulation of ~12 µM [68]. The swelling time was 45 min for lipid films and 90 min for precursor films. Swelling was performed at 4°C to slow actin polymerization and in a humid environment to prevent I-buffer evaporation. Liposomes were collected in an open-top observation chamber consisting of a spacer on a glass slide by pipetting 65 µl of a glucose solution (O-buffer) into the formation chamber and gently tilting it. We repeated this process twice, leading to at least a 2.6-fold dilution of actin remaining outside the liposomes. The observation chamber was closed by a coverslip. Glass slides and coverslips were passivated with a 2 mg/ml casein solution to prevent liposome adhesion and rupture. The liposomes were kept at 4°C for 5 – 10 min to ensure osmotic equilibrium between the interior and the external solution. Actin polymerization was initiated by bringing the observation chamber to room temperature and allowed to proceed for 45 min before observation.

Recently, it was shown that liposomes formed by swelling a hybrid film of agarose and lipids contain residual agarose [132]. We measured the fraction of residual agarose in our liposomes by measuring the fluorescence intensity of fluorescein-labeled agarose inside liposomes relative to the intensity in the swelling solution (containing 1 wt% of agarose), taking care to use the same illumination and image recording settings. We prepared fluorescein-labeled agarose according to the previously reported method [133]. In the absence of actin, the residual agarose content was 15% (average of 3 independent experiments, see Fig. S11). When actin and fascin were both present in the inner buffer, the residual agarose

content was 19% (Fig. S12*A*, *B*). Liposomes without protrusions had a slightly higher agarose content compared to protruded liposomes (Fig. S12*C*). However, the difference was small, so we do not expect that the residual agarose significantly affects liposome morphology. This interpretation is supported by additional control experiments where we prepared liposomes by swelling a hydrogel of polyvinyl alcohol (PVA), which does not get encapsulated [134]. We observed similar liposome morphologies of liposomes prepared by PVA swelling compared to agarose swelling (Fig. S13), indicating that residual agarose has a minor effect, if any, on liposome shape control by actin.

Control of membrane tension by osmolarity adjustment

Buffer osmolarities were measured by an Osmomat 030 osmometer (Gonotec GmbH, Berlin, Germany). The osmolarity difference between the I- and O-buffers was controlled by adjusting the glucose concentration in the O-buffer. In a hypertonic environment, where the O-buffer has a higher osmolarity than the I-buffer, the liposomes shrink: the osmolarity mismatch across the membrane sets up an outward flow of water that continues until osmotic equilibrium is reached. Assuming a fixed surface area, the liposome gains excess membrane area, ΔA, compared to a sphere of the same final volume. The relative area change is $\Delta A/A = 1 - [C_0/(C_0+\Delta C)]^{2/3}$, where A is the total liposome surface area, C_0 is the osmolarity of the I-buffer, and ΔC the osmotic gradient across the membrane [135]. In the calculation we neglected the presence of residual I-buffer outside liposomes.

Microscopy and image analysis

Confocal fluorescence and phase contrast images were taken on a Nikon Eclipse Ti inverted microscope equipped with a Nikon C1 confocal scanhead, a 100x/NA1.4 Plan Apo objective, and lasers with wavelengths of 488 nm and 543 nm. Images shown here are single confocal sections recorded at the equatorial plane of liposomes unless specified otherwise. Image analysis was performed with ImageJ software [136]. Liposomes with enclosed or adhered small liposomes, lipid aggregates, or tubes that could potentially affect membrane/actin morphology were excluded from the analysis (Fig. S14).

The actin shell thickness of a liposome was determined by integrating actin fluorescence intensity around concentric circles and repeating this for radial distances from the center of the liposome to its edge. By normalizing all values by the corresponding circumference (in pixels), we obtained a profile of integrated intensities along the liposome radius. To compare the integrated intensities of the liposome, we normalized integrated intensities by subtracting the minimum integrated intensity and then dividing by the difference between the maximum and minimum integrated intensities. The actin shell thickness was defined as the distance between the liposome edge and the radial position from the center of the liposome where the normalized integrated intensity is greater than 0.5. The shell thickness is finally divided by the liposome radius to obtain a normalized shell thickness. For a homogeneously filled liposome we expected a normalized shell thickness of 1. Since thick actin shells are in practice difficult to distinguish from homogeneous networks, we classified liposomes with a normalized shell thickness above 0.7 as "without cortical shell" and liposomes with normalized shell thicknesses below 0.7 as exhibiting a cortical shell.

For liposomes having no protrusion or in-plane protrusion(s), liposome shapes were quantified by manually detecting their 2D contour in the equatorial plane (*x*-*y* plane), using phase contrast or confocal fluorescence images. For liposomes with a membrane protrusion tilted out-of-plane, we determined the shape from an image obtained by summing several images along the *z*-axis from 3D confocal z-stacks. From the contours, we extracted two shape parameters: circularity and solidity [61]. *Circularity* is defined as the ratio of the area enclosed by the 2D contour over the area of a circle of equivalent perimeter; *solidity* is

defined as the ratio of the area enclosed by the contour over the area of its minimum convex hull. The width of a liposome body without the protruded part, called the main body, was obtained by fitting the body shape to an ellipse [136]. The minor (major) axis length of the ellipse was assigned to the body width (length) (Fig. S1*A*). The protrusion width was measured as an average of $2-3$ width values measured at different locations along the protrusion. For liposomes with more than one protrusion, we only presented the length of the longest protrusion in Figs. 6*A*, S2*B* and S4*E*.

The pixel-averaged intensity of actin bundles was determined by averaging line profiles along the bundles with a width of 1 pixel (0.05 – 0.22 μm/pixel, depending on image acquisition setting), and a length of at least 1.3 μm. The intensity was corrected for background noise by subtracting the average intensity of the dark background measured outside the liposomes. We measured the fluorescence intensity of the bundles relative to that of the background inside the liposome main body. The latter intensity was always significantly larger than the background intensity ((actin – background)/actin = 74 ± 15%), indicating the presence of encapsulated actin that was not incorporated in bundles. These results only provide us an estimate of the number of filaments per bundle, given that we could not distinguish between actin monomers and filaments.

To test the distribution of membrane lamellarities, we analyzed the membrane fluorescence intensity of the liposomes by manually drawing a line, with a width of 2 pixels and a length of at least 2 μm, along the contour of each liposome, followed by summing the fluorescence intensity values of all pixels within the line and normalizing by the number of pixels. The background fluorescence intensity, measured by the pixel-averaged fluorescence intensity inside a square area with a length about 1 μm outside of the corresponding liposomes, was then subtracted from the membrane fluorescence intensity.

Statistics

Scatter plots showed measurements for individual actin-fascin liposomes, collected from 2 experiments in each experimental condition. Notched boxes showed mean (small squares), maximum and minimum values (crosses), and the 5th and 95th (whiskers) and 25th and 75th percentile. The notches that extended to $\pm 1.58 \times IQR/\sqrt{N}$ (*IQR* is the interquartile range and *N* is the sample size) represented the 95% confidence level of the median value [137]. Statistical tests were performed by Pearson's linear correlation coefficient and the *p*-value was obtained from a Student's t-distribution.

Acknowledgements

We thank B. Stuhrmann, S. Roth, I. Garlea and B. Mulder for insightful discussions, M. Kuit-Vinkenoog, J. Alvarado, M. Preciado-López, S. Omar and L. Oppel for protein purification, and O. Mertins and C. Marques (Institut Charles Sadron, Strasbourg) for advice on the inverse phase precursor technique. Mouse fascin plasmid was a kind gift from S. Hansen and R.D. Mullins (UC San Francisco). This work was supported by a VIDI grant from the Netherlands Organization for Scientific Research (NWO) and by the Foundation for Fundamental Research on Matter (FOM), which is part of NWO.

References

[1] A. Pitaval, Q. Tseng, M. Bornens and M. Théry, *The Journal of cell biology*, 2010, **191**, 303–312.

[2] J. Fink, N. Carpi, T. Betz, A. Bétard, M. Chebah, A. Azioune, M. Bornens, C. Sykes, L. Fetler, D. Cuvelier *et al.*, *Nature cell biology*, 2011, **13**, 771–778.

[3] J. V. Small, T. Stradal, E. Vignal and K. Rottner, *Trends Cell Biol*, 2002, **12**, 112–120.

[4] T. M. Svitkina, *Current opinion in cell biology*, 2013.

[5] M. Krause and A. Gautreau, *Nat Rev Mol Cell Biol*, 2014, **15**, 577–590.

[6] P. K. Mattila and P. Lappalainen, *Nature Reviews Molecular Cell Biology*, 2008, **9**, 446–454.

[7] K. Kikuchi and K. Takahashi, *Cancer Sci*, 2008, **99**, 2252–2259.

[8] S. Rhee, H. Jiang, C.-H. Ho and F. Grinnell, *Proc Natl Acad Sci U S A*, 2007, **104**, 5425–5430.

[9] J. Alvarado, B. M. Mulder and G. H. Koenderink, *Soft Matter*, 2014.

[10] M. S. e Silva, J. Alvarado, J. Nguyen, N. Georgoulia, B. M. Mulder and G. H. Koenderink, *Soft Matter*, 2011, **7**, 10631–10641.

[11] M. C. Lagomarsino, C. Tanase, J. W. Vos, A. M. C. Emons, B. M. Mulder and M. Dogterom, *Biophysical journal*, 2007, **92**, 1046–1057.

[12] M. C. Lagomarsino, M. Dogterom and M. Dijkstra, *The Journal of chemical physics*, 2003, **119**, 3535–3540.

[13] S. Köster, J. Kierfeld and T. Pfohl, *The European Physical Journal E: Soft Matter and Biological Physics*, 2008, **25**, 439–449.

[14] H. T. McMahon and J. L. Gallop, *Nature*, 2005, **438**, 590–596.

[15] H. T. McMahon and E. Boucrot, *Journal of cell science*, 2015, **128**, 1065–1070.

[16] G. G. Borisy and T. M. Svitkina, *Current opinion in cell biology*, 2000, **12**, 104–112.

[17] R. Linck, X. Fu, J. Lin, C. Ouch, A. Schefter, W. Steffen, P. Warren and D. Nicastro, *Journal of Biological Chemistry*, 2014, jbc–M114.

[18] L. Tilney, *Journal of cell science*, 1968, **3**, 549–562.

[19] A. N. Schechter, *Blood*, 2008, **112**, 3927–3938.

[20] W. D. Cohen, Y. Sorokina and I. Sanchez, *Cell motility and the cytoskeleton*, 1998, **40**, 238–248.

[21] I. Nemhauser, J. Joseph-Silverstein and W. D. Cohen, *The Journal of cell biology*, 1983, **96**, 979–989.

[22] T. Asakura, J. A. Mattiello, K. Obata, K. Asakura, M. P. Reilly, N. Tomassini, E. Schwartz and K. Ohene-Frempong, *Proceedings of the National Academy of Sciences*, 1994, **91**, 12589–12593.

[23] J. D. Corbett, W. E. Mickols and M. F. Maestre, *Journal of Biological Chemistry*, 1995, **270**, 2708–2715.

[24] P. Sens and J. Plastino, *Journal of Physics: Condensed Matter*, 2015, **27**, 273103.

[25] K. Keren, *European Biophysics Journal*, 2011, **40**, 1013–1027.

[26] A. Diz-Muñoz, D. A. Fletcher and O. D. Weiner, *Trends in cell biology*, 2012.

[27] N. C. Gauthier, T. A. Masters and M. P. Sheetz, *Trends in cell biology*, 2012.

[28] K. Keren, Z. Pincus, G. M. Allen, E. L. Barnhart, G. Marriott, A. Mogilner and J. A. Theriot, *Nature*, 2008, **453**, 475–480.

[29] A. P. Liu, D. L. Richmond, L. Maibaum, S. Pronk, P. L. Geissler and D. A. Fletcher, *Nature physics*, 2008, **4**, 789–793.

[30] D. Marenduzzo and E. Orlandini, *EPL (Europhysics Letters)*, 2007, **80**, 48004.

[31] D. Marenduzzo, C. Micheletti and E. Orlandini, *Journal of Physics: Condensed Matter*, 2010, **22**, 283102.

[32] H. Lei and G. E. Karniadakis, *Soft matter*, 2012, **8**, 4507–4516.
[33] Z. Yang, D. Zhang, L. Zhang, C. Hongping, H. Liang *et al.*, *Soft Matter*, 2011, **7**, 6836–6843.
[34] M. Fošnaric, A. Iglic, D. M. Kroll and S. May, *Soft Matter*, 2013.
[35] M. Fritsche and D. W. Heermann, *Soft Matter*, 2011, **7**, 6906–6913.
[36] K. Ostermeir, K. Alim and E. Frey, *Physical Review E*, 2010, **81**, 061802.
[37] R. Morikawa, Y. Saito and H. Hyuga, *Journal of the Physical Society of Japan*, 1999, **68**, 1760–1768.
[38] T. Umeda, H. Nakajima and H. Hotani, *Journal of the Physics Society Japan*, 1998, **67**, 682–688.
[39] V. Heinrich, B. Božic, S. Svetina and B. Žekš, *Biophysical journal*, 1999, **76**, 2056–2071.
[40] W. Gózdz, *The Journal of Physical Chemistry B*, 2005, **109**, 21145–21149.
[41] M. Pinot, F. Chesnel, J. Z. Kubiak, I. Arnal, F. J. Nedelec and Z. Gueroui, *Current Biology*, 2009, **19**, 954–960.
[42] D. K. Fygenson, M. Elbaum, B. Shraiman and A. Libchaber, *Physical Review E*, 1997, **55**, 850.
[43] L. Blanchoin, R. Boujemaa-Paterski, C. Sykes and J. Plastino, *Physiological reviews*, 2014, **94**, 235–263.
[44] A. Kapus and P. Janmey, *Comprehensive Physiology*, 2013.
[45] M. M. Claessens, M. Bathe, E. Frey and A. R. Bausch, *Nature materials*, 2006, **5**, 748–753.
[46] L. Limozin, M. Bärmann and E. Sackmann, *The European Physical Journal E: Soft Matter and Biological Physics*, 2003, **10**, 319–330.
[47] M. Claessens, R. Tharmann, K. Kroy and A. Bausch, *Nature Physics*, 2006, **2**, 186–189.
[48] F. Gittes, B. Mickey, J. Nettleton and J. Howard, *The Journal of cell biology*, 1993, **120**, 923–934.
[49] O. Lieleg, K. M. Schmoller, C. J. Cyron, Y. Luan, W. A. Wall and A. R. Bausch, *Soft Matter*, 2009, **5**, 1796–1803.
[50] L. Limozin and E. Sackmann, *Physical review letters*, 2002, **89**, 168103.
[51] M. Honda, K. Takiguchi, S. Ishikawa and H. Hotani, *Journal of molecular biology*, 1999, **287**, 293–300.
[52] M. J. Footer, J. W. Kerssemakers, J. A. Theriot and M. Dogterom, *Proceedings of the National Academy of Sciences*, 2007, **104**, 2181–2186.
[53] D. R. Kovar and T. D. Pollard, *Proceedings of the National Academy of Sciences of the United States of America*, 2004, **101**, 14725–14730.
[54] E. Atilgan, D. Wirtz and S. X. Sun, *Biophysical journal*, 2006, **90**, 65–76.
[55] S. Pronk, P. L. Geissler and D. A. Fletcher, *Physical review letters*, 2008, **100**, 258102.
[56] A. Mogilner and B. Rubinstein, *Biophysical journal*, 2005, **89**, 782–795.
[57] D. J. DeRosier and K. T. Edds, *Experimental cell research*, 1980, **126**, 490–494.
[58] D. Vignjevic, S.-i. Kojima, Y. Aratyn, O. Danciu, T. Svitkina and G. G. Borisy, *The Journal of cell biology*, 2006, **174**, 863–875.
[59] Y. S. Aratyn, T. E. Schaus, E. W. Taylor and G. G. Borisy, *Molecular biology of the cell*, 2007, **18**, 3928–3940.
[60] R. Ishikawa, T. Sakamoto, T. Ando, S. Higashi-Fujime and K. Kohama, *Journal of neurochemistry*, 2003, **87**, 676–685.
[61] M. Yang, K. Kpalma, J. Ronsin *et al.*, *Pattern recognition*, 2008, 43–90.

[62] D. Strehle, J. Schnauß, C. Heussinger, J. Alvarado, M. Bathe, J. Käs and B. Gentry, *European Biophysics Journal*, 2011, **40**, 93–101.
[63] Y. Tseng, E. Fedorov, J. M. McCaffery, S. C. Almo and D. Wirtz, *Journal of molecular biology*, 2001, **310**, 351–366.
[64] N. Leijnse, L. B. Oddershede and P. M. Bendix, *Proceedings of the National Academy of Sciences*, 2015, **112**, 136–141.
[65] K. Carvalho, F.-C. Tsai, E. Lees, R. Voituriez, G. Koenderink and C. Sykes, *Proceedings of the National Academy of Sciences*, 2013, **110**, 16456–16461.
[66] L. Landau and E. Lifshitz, *Theory of Elasticity, 3rd*, 1986.
[67] M. Claessens, C. Semmrich, L. Ramos and A. Bausch, *Proceedings of the National Academy of Sciences*, 2008, **105**, 8819–8822.
[68] F.-C. Tsai, B. r. Stuhrmann and G. H. Koenderink, *Langmuir*, 2011, **27**, 10061–10071.
[69] S. Dieluweit, A. Csisza r, W. Rubner, J. Fleischhauer, S. Houben and R. Merkel, *Langmuir*, 2010, **26**, 11041–11049.
[70] W. Helfrich, *Zeitschrift für Naturforschung. Teil C: Biochemie, Biophysik, Biologie, Virologie*, 1973, **28**, 693.
[71] T. M. Svitkina, E. A. Bulanova, O. Y. Chaga, D. M. Vignjevic, S.-i. Kojima, J. M. Vasiliev and G. G. Borisy, *The Journal of cell biology*, 2003, **160**, 409–421.
[72] K.-i. Akashi, H. Miyata, H. Itoh and K. Kinosita Jr, *Biophysical journal*, 1996, **71**, 3242–3250.
[73] B. Bozic, S. Svetina and B. Zeks, *Physical Review E*, 1997, **55**, 5834.
[74] C. S. Peskin, G. M. Odell and G. F. Oster, *Biophysical Journal*, 1993, **65**, 316–324.
[75] T. Kaneko, T. J. Itoh and H. Hotani, *Journal of molecular biology*, 1998, **284**, 1671–1681.
[76] D. K. Fygenson, J. F. Marko and A. Libchaber, *Physical review letters*, 1997, **79**, 4497–4500.
[77] M. Elbaum, D. Kuchnir Fygenson and A. Libchaber, *Physical review letters*, 1996, **76**, 4078–4081.
[78] V. Emsellem, O. Cardoso and P. Tabeling, *Physical Review E*, 1998, **58**, 4807–4810.
[79] H. Hotani and H. Miyamoto, *Advances in biophysics*, 1990, **26**, 135–156.
[80] A. Roux, *Soft Matter*, 2013.
[81] W. Rawicz, K. Olbrich, T. McIntosh, D. Needham and E. Evans, *Biophysical Journal*, 2000, **79**, 328–339.
[82] T. R. Powers, G. Huber and R. E. Goldstein, *Physical Review E*, 2002, **65**, 041901.
[83] I. Derényi, F. Jülicher and J. Prost, *Physical review letters*, 2002, **88**, 238101.
[84] G. Koster, A. Cacciuto, I. Derényi, D. Frenkel and M. Dogterom, *Physical review letters*, 2005, **94**, 068101.
[85] T. D. Pollard, L. Blanchoin and R. D. Mullins, *Annual review of biophysics and biomolecular structure*, 2000, **29**, 545–576.
[86] H. Miyata and H. Hotani, *Proceedings of the National Academy of Sciences*, 1992, **89**, 11547–11551.
[87] H. Miyata, S. Nishiyama, K.-i. Akashi and K. Kinosita Jr, *Proceedings of the National Academy of Sciences*, 1999, **96**, 2048–2053.
[88] J. D. Cortese, B. Schwab, C. Frieden, E. L. Elson *et al.*, *Proceedings of the National Academy of Sciences*, 1989, **86**, 5773–5777.
[89] P. A. Janmey, C. C. Cunningham, G. F. Oster and T. P. Stossel, *NATO ASI SERIES H CELL BIOLOGY*, 1992, 333–333.
[90] H. Maemichi, K. Shikinaka, A. Kakugo, H. Furukawa, Y. Osada and J. P. Gong, *Langmuir*, 2008, **24**, 11975–11981.

[91] O. Medalia, M. Beck, M. Ecke, I. Weber, R. Neujahr, W. Baumeister and G. Gerisch, *Current biology*, 2007, **17**, 79–84.
[92] D. R. Daniels and M. S. Turner, *PloS one*, 2013, **8**, e59010.
[93] A. Husainy, A. Morrow, T. Perkins and J. Lee, *BMC cell biology*, 2010, **11**, 86.
[94] W. Wood and P. Martin, *The international journal of biochemistry & cell biology*, 2002, **34**, 726–730.
[95] T. Gustafson and L. Wolpert, *Experimental cell research*, 1961, **24**, 64–79.
[96] G. Orly, M. Naoz and N. Gov, *Biophysical journal*, 2014, **107**, 576–587.
[97] P. Bucher, A. Fischer, P. L. Luisi, T. Oberholzer and P. Walde, *Langmuir*, 1998, **14**, 2712–2721.
[98] Y. Lan and G. A. Papoian, *Biophysical journal*, 2008, **94**, 3839–3852.
[99] M. Bathe, C. Heussinger, M. M. Claessens, A. R. Bausch and E. Frey, *Biophysical journal*, 2008, **94**, 2955–2964.
[100] T. Bornschlögl, *Cytoskeleton*, 2013, **70**, 590–603.
[101] A. W. Schaefer, N. Kabir and P. Forscher, *The Journal of cell biology*, 2002, **158**, 139–152.
[102] H. Kress, E. H. Stelzer, D. Holzer, F. Buss, G. Griffiths and A. Rohrbach, *Proceedings of the National Academy of Sciences*, 2007, **104**, 11633–11638.
[103] L. G. Tilney and S. Inoué, *The Journal of cell biology*, 1982, **93**, 820–827.
[104] D. Daniels, *Biophysical journal*, 2010, **98**, 1139–1148.
[105] C. Yang and T. Svitkina, *Cell adhesion & migration*, 2011, **5**, 402–408.
[106] M. Barzik, L. M. McClain, S. L. Gupton and F. B. Gertler, *Molecular biology of the cell*, 2014, **25**, 2604–2619.
[107] R. Jaiswal, D. Breitsprecher, A. Collins, I. R. Corrêa, M.-Q. Xu and B. L. Goode, *Current Biology*, 2013, **23**, 1373–1379.
[108] K. Lee, J. L. Gallop, K. Rambani and M. W. Kirschner, *Science*, 2010, **329**, 1341–1345.
[109] A. Disanza, S. Bisi, M. Winterhoff, F. Milanesi, D. S. Ushakov, D. Kast, P. Marighetti, G. Romet-Lemonne, H.-M. Müller, W. Nickel *et al.*, *The EMBO journal*, 2013, **32**, 2735–2750.
[110] D. J. Kast, C. Yang, A. Disanza, M. Boczkowska, Y. Madasu, G. Scita, T. Svitkina and R. Dominguez, *Nature structural & molecular biology*, 2014, **21**, 413–422.
[111] A. Disanza, S. Mantoani, M. Hertzog, S. Gerboth, E. Frittoli, A. Steffen, K. Berhoerster, H.-J. Kreienkamp, F. Milanesi, P. P. Di Fiore *et al.*, *Nature cell biology*, 2006, **8**, 1337–1347.
[112] K. Wolff, C. Barrett-Freeman, M. R. Evans, A. B. Goryachev and D. Marenduzzo, *Physical biology*, 2014, **11**, 016005.
[113] S. A. Sinnar, S. Antoku, J.-M. Saffin, J. A. Cooper and S. Halpain, *Molecular biology of the cell*, 2014, **25**, 2152–2160.
[114] T. M. Watanabe, H. Tokuo, K. Gonda, H. Higuchi and M. Ikebe, *Journal of Biological Chemistry*, 2010, **285**, 19605–19614.
[115] L.-L. Pontani, J. Van der Gucht, G. Salbreux, J. Heuvingh, J.-F. Joanny and C. Sykes, *Biophysical journal*, 2009, **96**, 192–198.
[116] Y. Ideses, Y. Brill-Karniely, L. Haviv, A. Ben-Shaul and A. Bernheim-Groswasser, 2008.
[117] J. Saarikangas, N. Kourdougli, Y. Senju, G. Chazal, M. Segerstråle, R. Minkeviciene, J. Kuurne, P. K. Mattila, L. Garrett, S. M. Hölter *et al.*, *Developmental cell*, 2015.
[118] H. Zhao, A. Pykäläinen and P. Lappalainen, *Current opinion in cell biology*, 2011, **23**, 14–21.
[119] C. Yang, M. Hoelzle, A. Disanza, G. Scita and T. Svitkina, *PloS one*, 2009, **4**, e5678.

[120] H. Isambert, P. Venier, A. C. Maggs, A. Fattoum, R. Kassab, D. Pantaloni and M.-F. Carlier, *Journal of Biological Chemistry*, 1995, **270**, 11437–11444.
[121] G. Morrison and D. Thirumalai, *Physical Review E*, 2009, **79**, 011924.
[122] J. G. White and J. J. Sauk, *Blood*, 1984, **64**, 470–478.
[123] S. Patel-Hett, J. L. Richardson, H. Schulze, K. Drabek, N. A. Isaac, K. Hoffmeister, R. A. Shivdasani, J. C. Bulinski, N. Galjart, J. H. Hartwig *et al.*, *Blood*, 2008, **111**, 4605–4616.
[124] M. Mishra, J. Kashiwazaki, T. Takagi, R. Srinivasan, Y. Huang, M. K. Balasubramanian and I. Mabuchi, *Nature cell biology*, 2013, **15**, 853–859.
[125] M. Miyazaki, M. Chiba, H. Eguchi, T. Ohki and S. Ishiwata, *Nature cell biology*, 2015.
[126] M. Mavrakis, Y. Azou-Gros, F.-C. Tsai, J. Alvarado, A. Bertin, F. Iv, A. Kress, S. Brasselet, G. H. Koenderink and T. Lecuit, *Nature cell biology*, 2014, **16**, 322–334.
[127] B. S. Gentry, S. van der Meulen, P. Noguera, B. Alonso-Latorre, J. Plastino and G. H. Koenderink, *European Biophysics Journal*, 2012, **41**, 979–990.
[128] S. Ishiwata, *Journal of biochemistry*, 1976, **80**, 595–609.
[129] J. X. Tang, P. A. Janmey, T. P. Stossel and T. Ito, *Biophysical journal*, 1999, **76**, 2208–2215.
[130] M. Carlier, D. Pantaloni and E. D. Korn, *Journal of Biological Chemistry*, 1985, **260**, 6565–6571.
[131] O. Mertins, N. P. da Silveira, A. R. Pohlmann, A. P. Schröder and C. M. Marques, *Biophysical journal*, 2009, **96**, 2719–2726.
[132] R. B. Lira, R. Dimova and K. A. Riske, *Biophysical journal*, 2014, **107**, 1609–1619.
[133] K. Horger, D. Estes, R. Capone and M. Mayer, *Journal of the American Chemical Society*, 2009, **131**, 1810–1819.
[134] A. Weinberger, F.-C. Tsai, G. H. Koenderink, T. F. Schmidt, R. Itri, W. Meier, T. Schmatko, A. Schröder and C. Marques, *Biophysical journal*, 2013, **105**, 154–164.
[135] M. Claessens, F. Leermakers, F. Hoekstra and M. Stuart, *Biochimica et Biophysica Acta (BBA)-Biomembranes*, 2008, **1778**, 890–895.
[136] J. Schindelin, I. Arganda-Carreras, E. Frise, V. Kaynig, M. Longair, T. Pietzsch, S. Preibisch, C. Rueden, S. Saalfeld, B. Schmid *et al.*, *Nature methods*, 2012, **9**, 676–682.
[137] R. McGill, J. W. Tukey and W. A. Larsen, *The American Statistician*, 1978, **32**, 12–16.

Figures

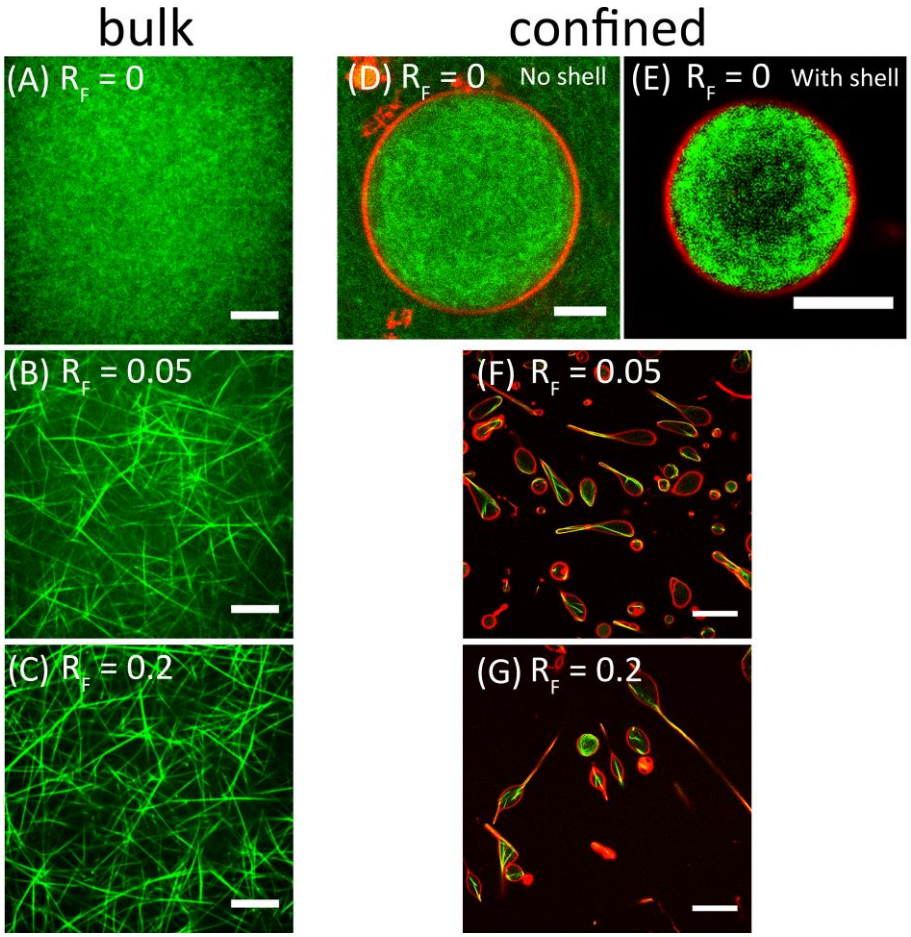

FIGURE 1 Confocal images of actin networks polymerized in bulk solution (*A*-*C*) and confined inside cell-sized liposomes (*D*-*G*). (*A*-*C*) Bulk actin networks formed in the absence (*A*) and presence (*B* and *C*) of fascin. (*D*-*G*). Actin networks inside liposomes formed in the absence (*D* and *E*) and presence (*F* and *G*) of fascin. R_F indicates the molar ratio of fascin to actin. Actin concentrations: (*A*-*C*) 12 μM and (*D*-*G*) 23.8 μM in the swelling solution (after encapsulation, ~12 μM is present inside the liposomes [68]). Actin is shown in green and lipid membranes in red. Scale bars: (*A*-*C*) 10 μm, (*D* and *E*) 5 μm, (*F* and *G*) 20 μm.

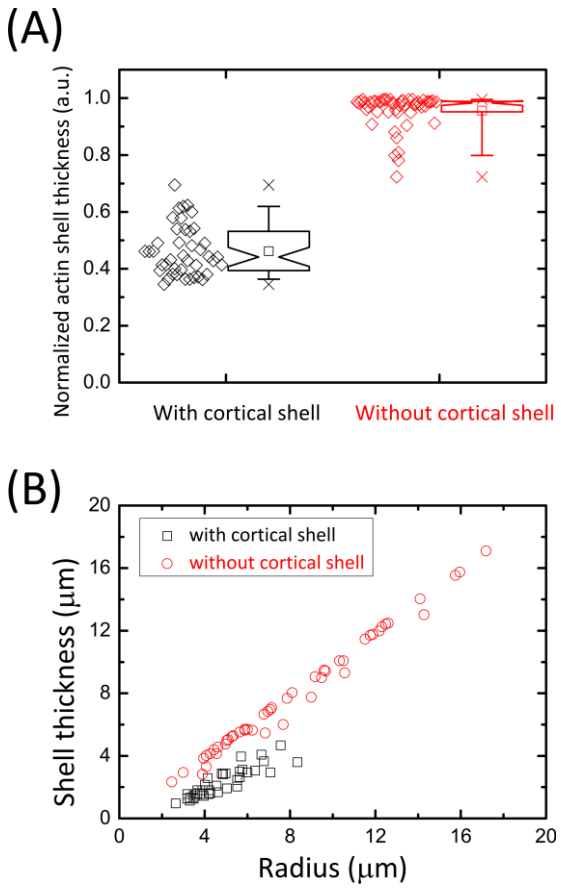

FIGURE 2 Confinement-induced cortical shell formation of actin filaments encapsulated in liposomes in the absence of fascin. (*A*) Actin fluorescence signals along liposome radius normalized by the corresponding liposome radius (see Material and Method for detail). A liposome is classified as exhibiting an cortical shell *("with cortical shell"*) if its normalized shell thickness is below 0.7, otherwise it is classified as "*without cortical shell*". Liposome population sizes: 42 (*with cortical shell*) and 50 (*without cortical shell*). (*B*) Dependence of actin shell thickness on liposome radius. Note that actin shells are only found in liposomes with a radius below 8 μm, indicating that confinement promotes shell formation.

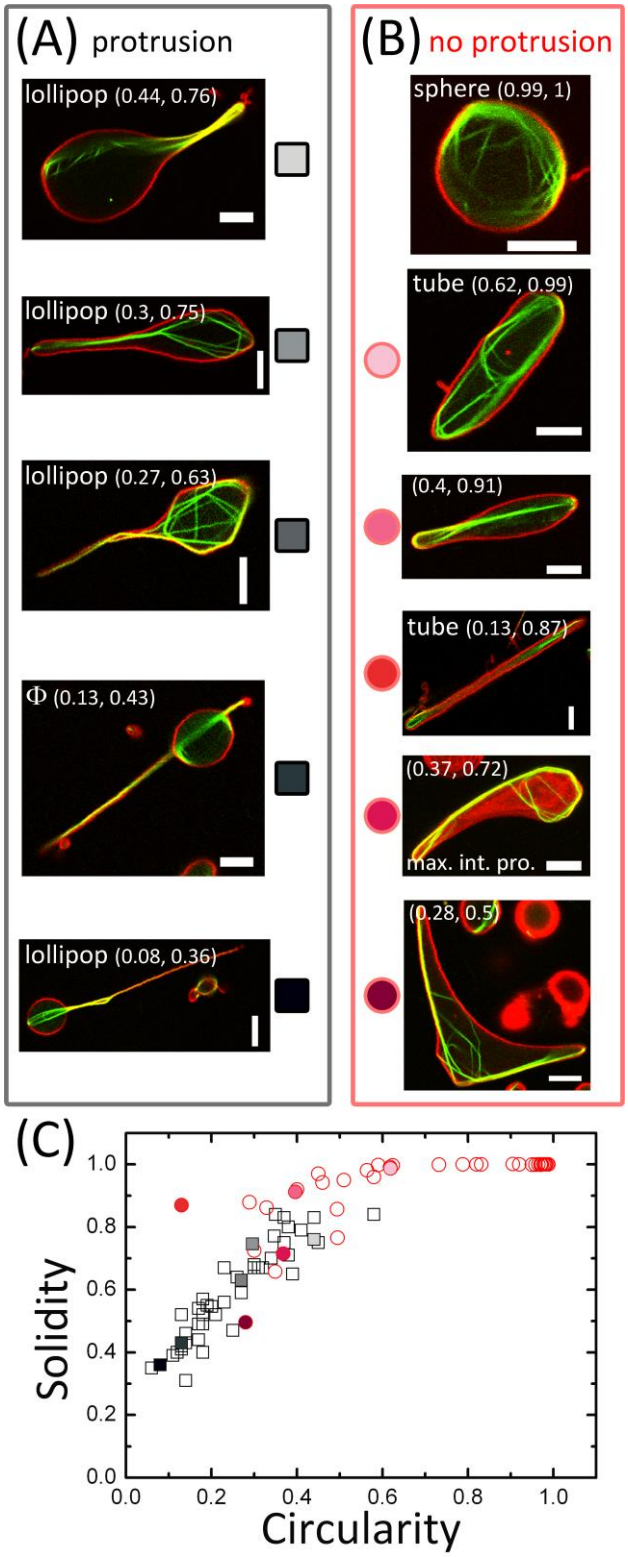

FIGURE 3 Morphological characterization of liposomes encapsulating actin-fascin bundles (R_F = 0.05). (*A*, *B*) Typical confocal fluorescence images of liposomes sorted by the extent of membrane deformation (increasing from *top* to *bottom*). The panel with (circularity, solidity) = (0.37, 0.72) in (*B*) shows a maximum intensity projection (*max. int. pro.*) of 11 planes over a z-range of 5 μm. Red: membrane, green: actin. Scale bars: 5 μm. (*C*) Summary of all observed liposome shapes in terms of circularity and solidity. Reddish symbols represent liposomes having no protrusion (42 liposomes) and black/grayish symbols are liposomes with one or more protrusions (45 liposomes). Color-coded solid symbols correspond to the confocal images as labeled.

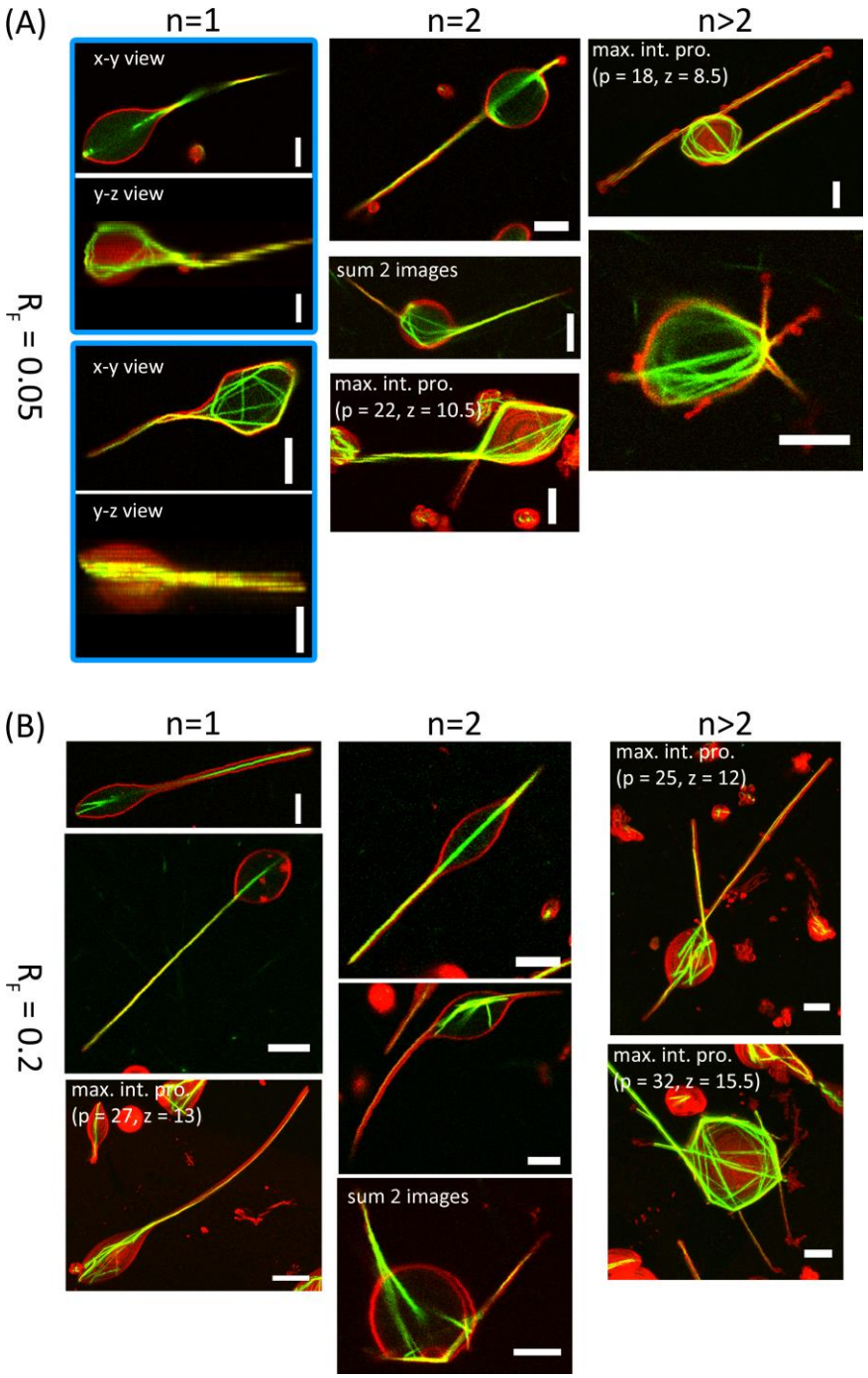

FIGURE 4 Confocal fluorescence images of typical liposomes with a single (n = 1) and multiple (n = 2 and n > 2) protrusions at low (*A*) and high (*B*) fascin-to-actin molar ratio, R_F. In the middle image in (*A*) n = 2 and the bottom image in (*B*) n = 2, two confocal images are summed to show the entire shape, labelled *sum 2 images*. Images labelled *max. int. pro*. represent maximum intensity projections constructed from a confocal stack of p planes over a range z (in μm). Scale bars: 5 μm, except for the bottom image in (*B*) n = 1 where the scale bar is 10 μm. Red: membrane, green: actin.

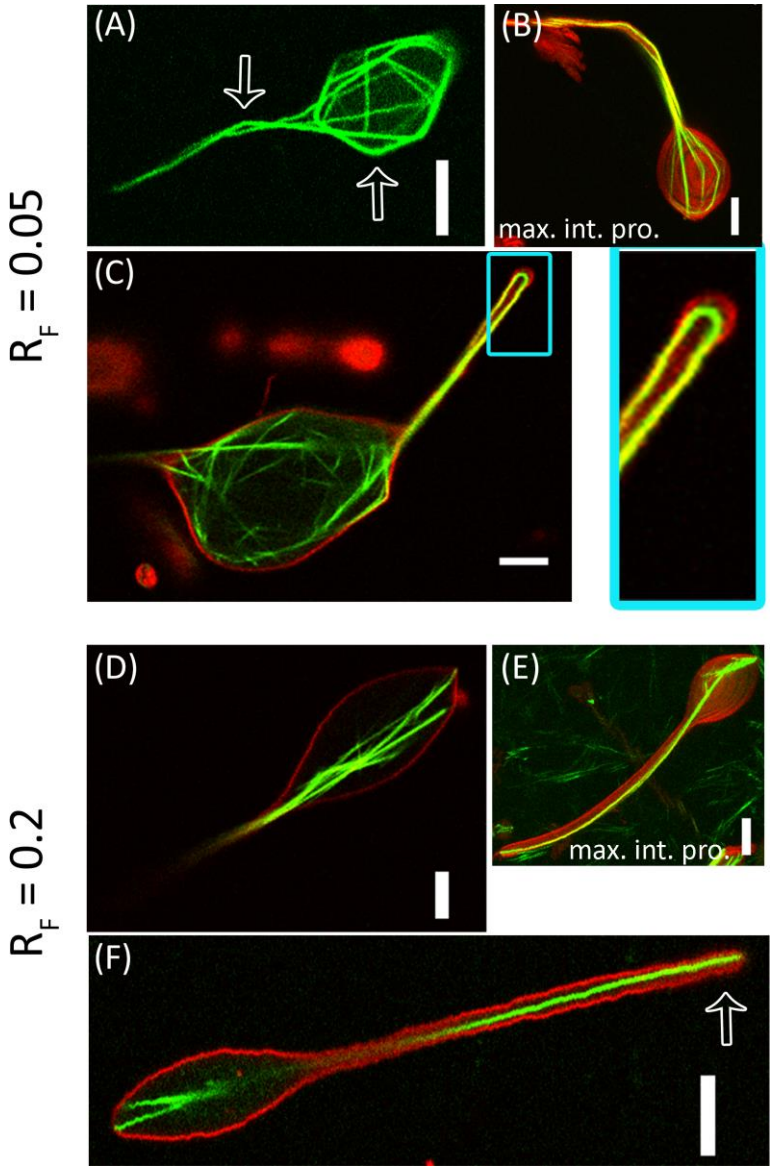

FIGURE 5 Characterization of actin-fascin bundles inside liposomes at low (*A* – *C*: R_F = 0.05) and high (*D* – *F*: R_F = 0.2) fascin-to-actin molar ratio, R_F. At R_F = 0.05, the actin bundles are softer and tend to exhibit kinks in the liposome main body (*A*) and in the protrusions (*A* and *B*), see arrows. Bundles sometimes buckle at the end of a protrusion (*C*, *blue box* and enlarged *blue rectangular area* on the *right panel*). By contrast, at R_F = 0.2, the actin bundles are more rigid and are straight inside the liposome main body (*D*), only occasionally gently curved along a protrusion (*E*), and always straight at the end of a protrusion (*F*, arrow). In (*B*) and (*E*) maximum intensity projections (*max. int. pro.*) are assembled from 25 planes over a total z-range of 12 μm in (*B*) and 21 planes over a total z-range of 10 μm in (*E*). Red: Membrane, green: actin. Scale bars: 5 μm.

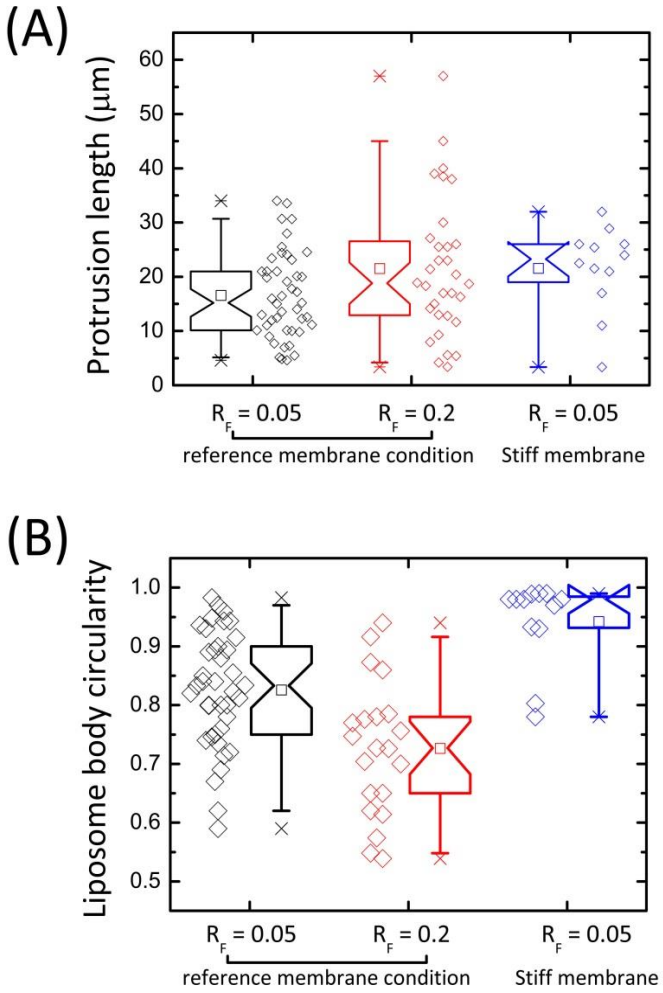

FIGURE 6 (*A*) Dependence of membrane protrusion length on actin bundle stiffness (tuned by the fascin-to-actin molar ratio, R_F) and membrane stiffness (around 10 k_BT for the reference membrane condition and ca. 10-fold stiffer for the *stiff membrane* condition [69]). Liposome population sizes from left to right: 45, 32 and 12. (*B*) Circularity of the main body of liposomes exhibiting a single protrusion. Liposome population sizes from left to right: 39, 21 and 12.

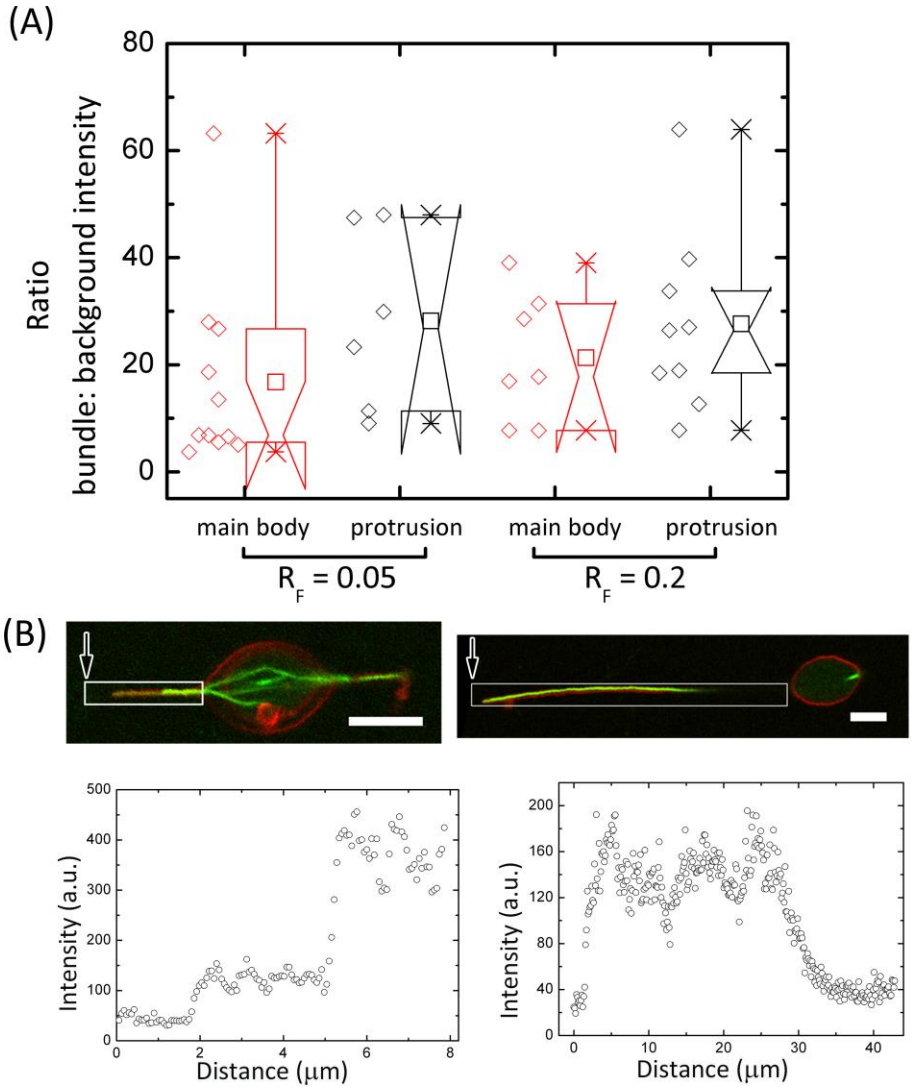

FIGURE 7 (*A*) Actin bundle thickness quantified by the fluorescence intensity of actin bundles relative to that of the background actin signal in liposome main body. Liposome population sizes from left to right: 11, 6, 7, 9. (*B*) Example intensity profiles of actin bundles. *Top*: confocal images of liposomes at R_F = 0.2. Red: membrane, green: actin. Scale bars: 5 μm. *Bottom*: fluorescence intensities are calculated along the actin bundles within the *white boxes* in the images. The *x*-axis shows the horizontal distance, starting from the left (*white arrows* in the images); the *y*-axis shows intensities obtained by integrating along the vertical direction for each horizontal pixel position, followed by averaging by the vertical pixel length.

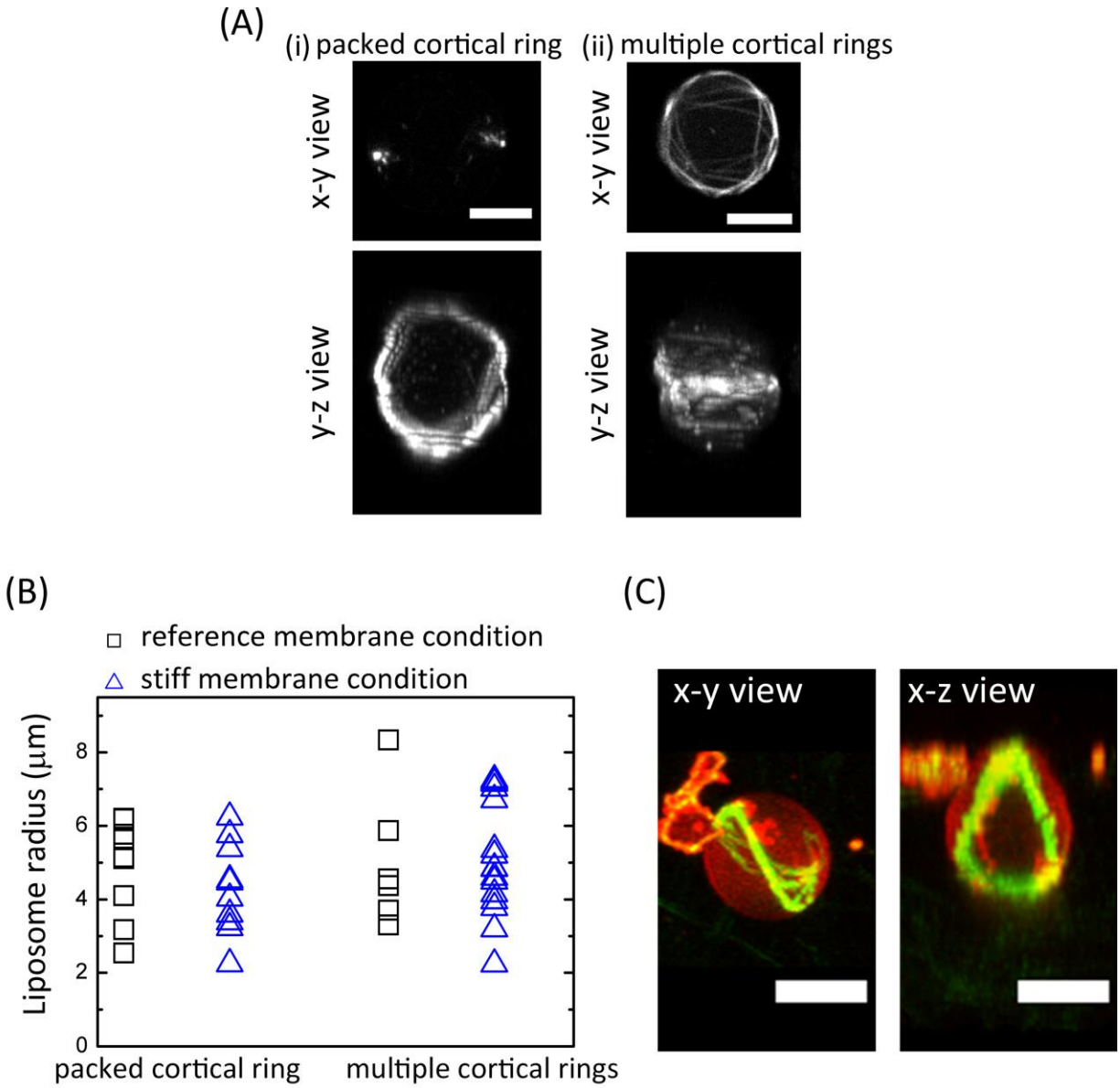

FIGURE 8 Organization of actin-fascin bundles confined in non-protruded liposomes at R_F = 0.05. (*A*) *Top*: confocal images of actin-fascin bundles inside liposomes (x-y view). *Bottom*: Orthogonal side views obtained by generating maximum intensity projections from confocal z-stacks along the y-z direction (y-z view). The "*stiff membrane*" liposomes exhibit either a packed cortical ring composed of actin bundles (*i*), or multiple cortical rings (*ii*). (*B*) Radius of liposomes containing packed or multiple cortical rings. Radii represent the equivalent radius of a circle having the same cross-sectional area as the liposome at its equatorial plane. Liposome population sizes from *left* to *right*: 11, 10, 6 and 18. (*C*) Two orthogonal side views obtained by generating maximum intensity projections from confocal z-stacks along the x-y and x-z directions. The "*stiff membrane*" liposome contains a twisted ring-like bundle structure. Red: membrane, green: actin. Scale bars: 5 μm.

Supplementary Material

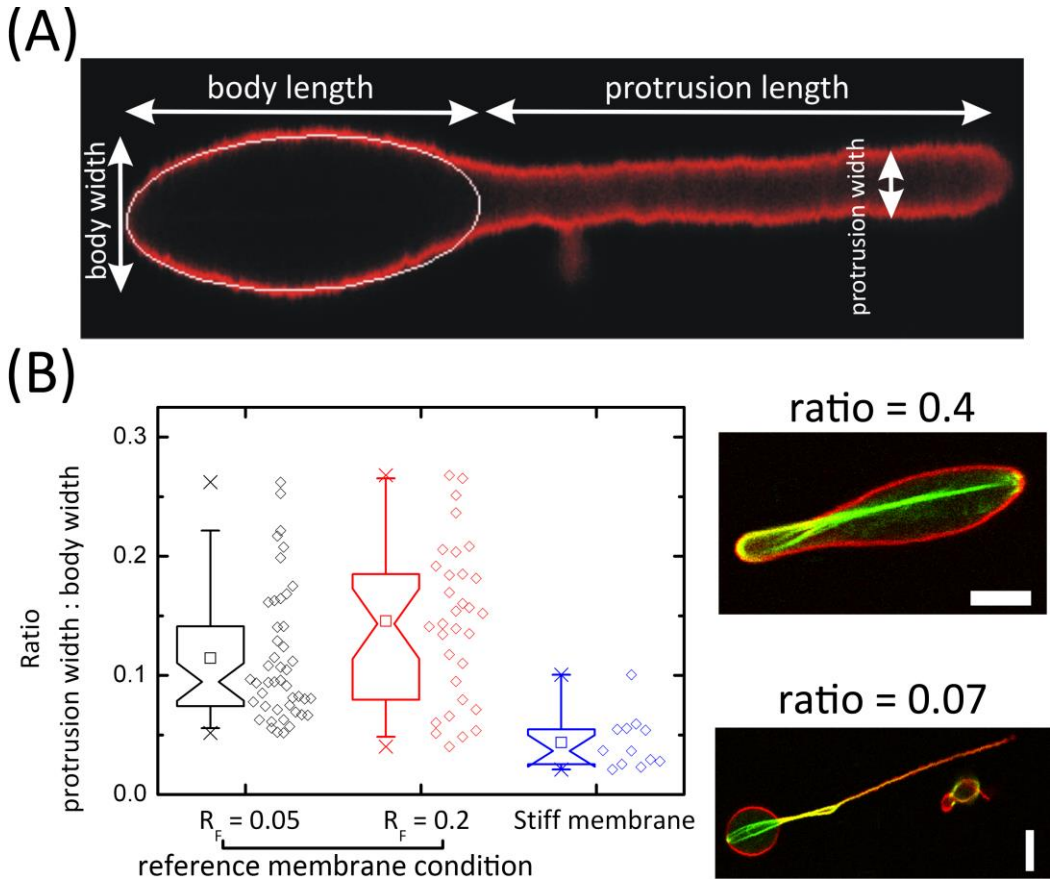

FIGURE S1 (*A*) Confocal image of a deformed liposome in which the white ellipse presents the result of fitting its main body contour to an ellipse and the white arrows indicate the lengths and widths of the body and the protrusion. (B) *Left*: Distributions of protrusion-to-body width ratios observed for actin-filled liposomes prepared under different conditions as labeled. Note that only liposomes having a protrusion-to-body width ratio below 0.3 are classified as "*protruded liposomes*" and are shown here. Liposome population sizes from left to right: 45, 32 and 12. *Right*: Confocal fluorescence images show a liposome classified as having no protrusion (*top panel*, protrusion-to-body width ratio = 0.4) and a liposome classified as having a protrusion (*bottom panel*, protrusion-to-body width ratio = 0.07). Red: membrane, green: actin. Scale bars: 5 μm.

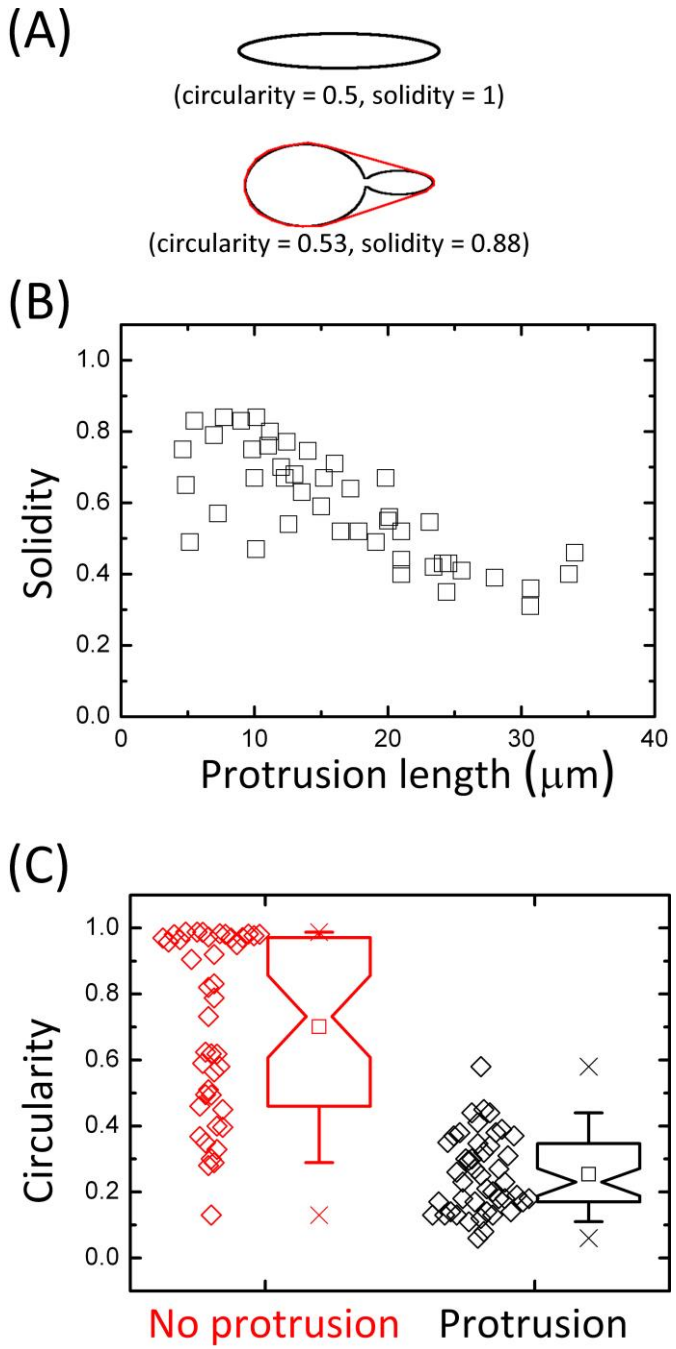

FIGURE S2 Morphological characterization of liposomes encapsulating actin-fascin bundles at R_F = 0.05. (*A*) *Top*: circularity quantifies the deviation of a liposome shape from a circle. *Bottom*: solidity quantifies the degree of concavity of a liposome shape by comparing its area to that of a convex hull enclosing the shape, shown by the red line. Solidity and circularity range from 1 (for a circle) to 0. (*B*) The liposome solidity is inversely correlated with the protrusion length (correlation coefficient = -0.772, p <0.001). (*C*) Comparison of circularities of liposomes with (45 liposomes) and without (42 liposomes) protrusions.

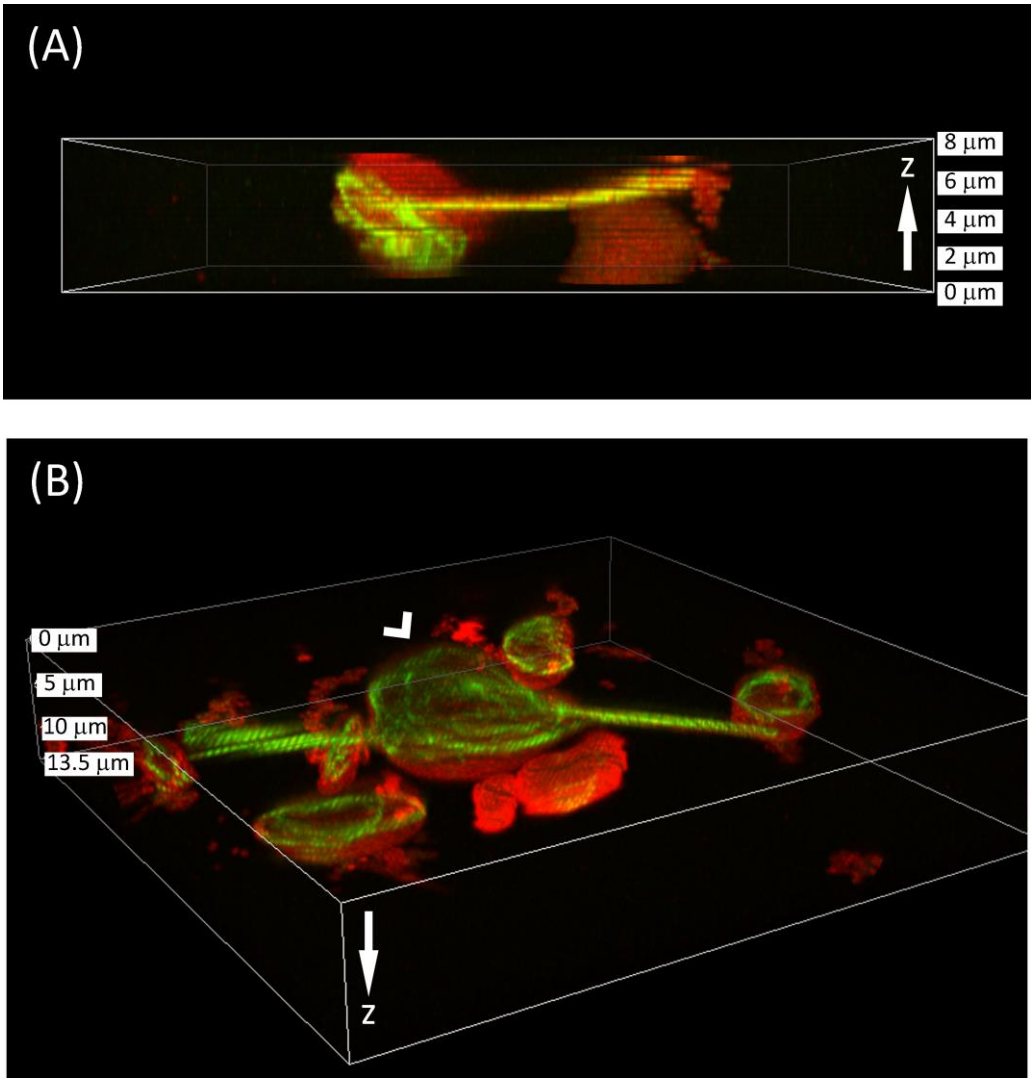

FIGURE S3 3D reconstructions of confocal fluorescence z-stacks obtained for liposomes encapsulating actin-fascin bundles. (*A*) A planar ring-like actin bundle structure in a protruded liposome. (*B*) Multiple ring-like structures of actin bundles (indicated by the white arrow head) inside a protruded liposome with two protrusions. Liposomes were formed at the *reference membrane* condition and with $R_F = 0.05$. Note that the smaller structures around the liposome are small liposomes. Red: membrane, green: actin.

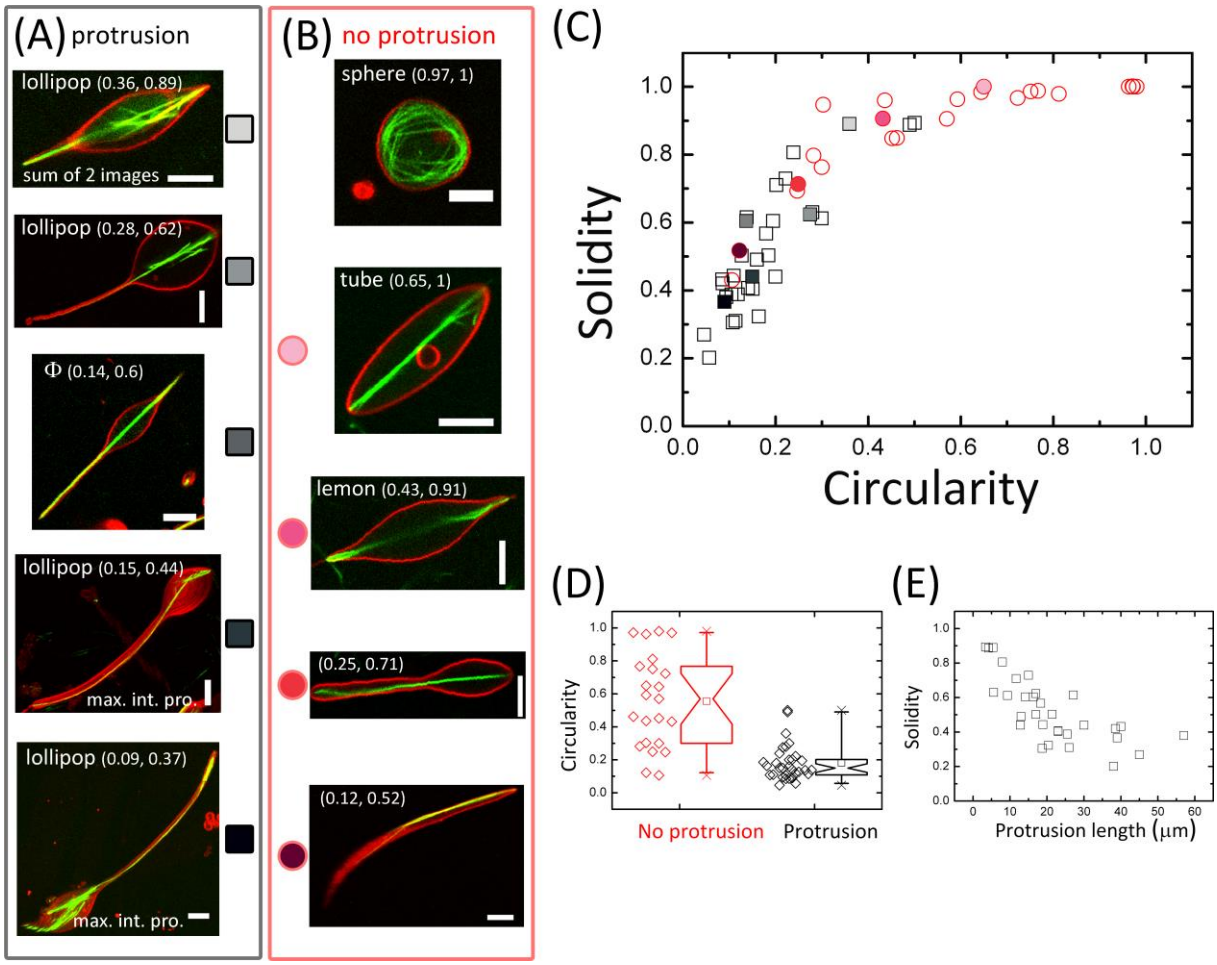

FIGURE S4 Morphological characterization of a population of 55 liposomes encapsulating stiff actin-fascin bundles (R_F = 0.2). (*A* and *B*) Confocal images of liposomes that are increasingly deformed (*top* to *bottom*). Images are single confocal sections recorded at the equatorial plane of the liposomes, except for the lollipop (0.36, 0.89), where 2 confocal images are summed to show the entire shape (*sum of 2 images*), and for the lollipop (0.15, 0.44) and (0.09, 0.37), where maximum intensity projections (*max. int. pro.*) are shown composed of *p* planes over a total z-range (*z* in μm) of (*p* = 21, *z* = 10) and (*p* = 22, *z* = 10.5), respectively. Red: membrane, green: actin. Scale bars: 5 μm. (*C*) The broad range of liposome shapes can be summarized in terms of circularity and solidity. Reddish symbols represent liposomes having no protrusion (23 liposomes) and black/grayish symbols represent liposomes with one or more protrusions (32 liposomes). Color-coded solid symbols correspond to images of liposomes in (*A*) and (*B*). (*D*) Circularities of liposomes with and without protrusions. Similar to the liposomes formed at low R_F, protruded liposomes have a lower circularity than most non-protruded liposomes. (*E*) The solidity is inversely correlated with the protrusion length (correlation coefficient = -0.724, $p < 0.001$).

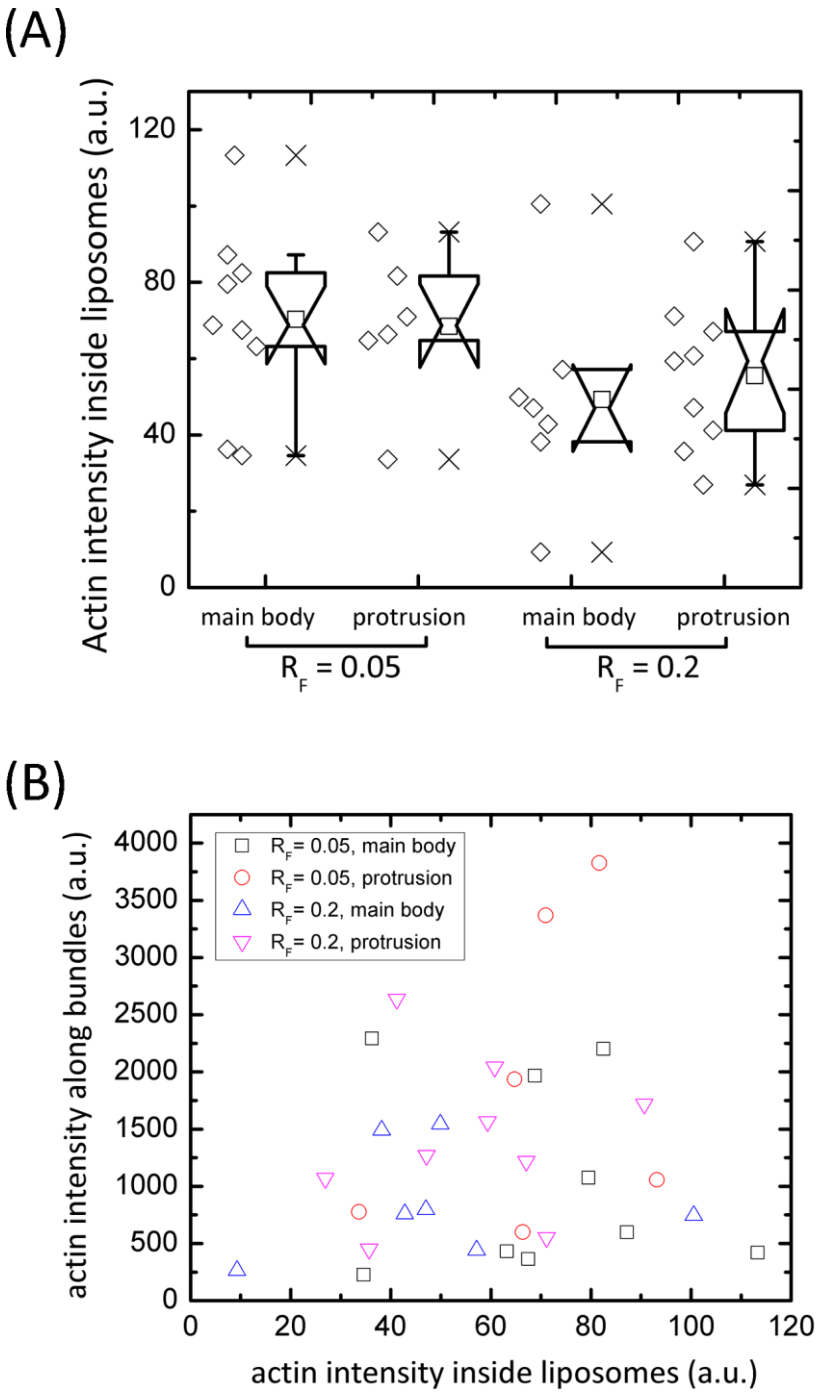

FIGURE S5 (A) Fluorescence intensity of unbundled actin inside liposomes. Liposome population sizes from *left* to *right*: 9, 6, 7, 9. (B) There is no correlation between the fluorescence intensities of actin bundles and of unbundled actin in each liposome (correlation coefficient = 0.1258, p = 0.5001).

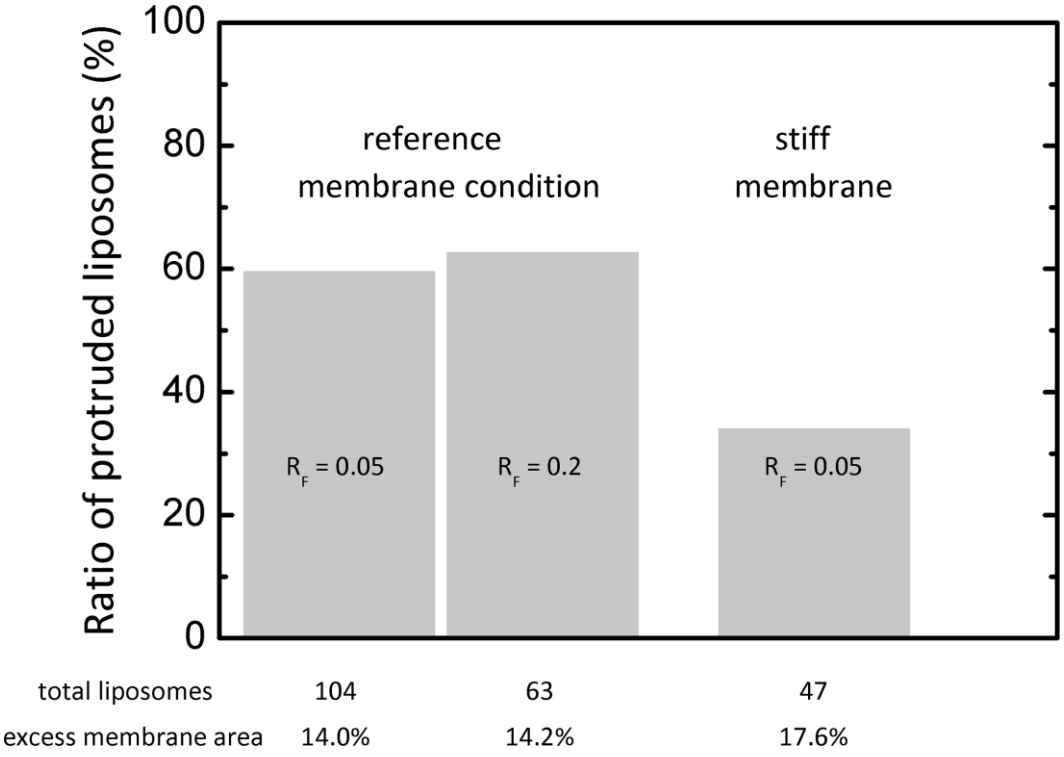

FIGURE S6 Membrane bending rigidity affects the likelihood of membrane protrusion formation. In all cases, the membranes are floppy with an estimated excess membrane area of 14-17%. At the *stiff membrane* condition, the membrane is decorated with neutravidin.

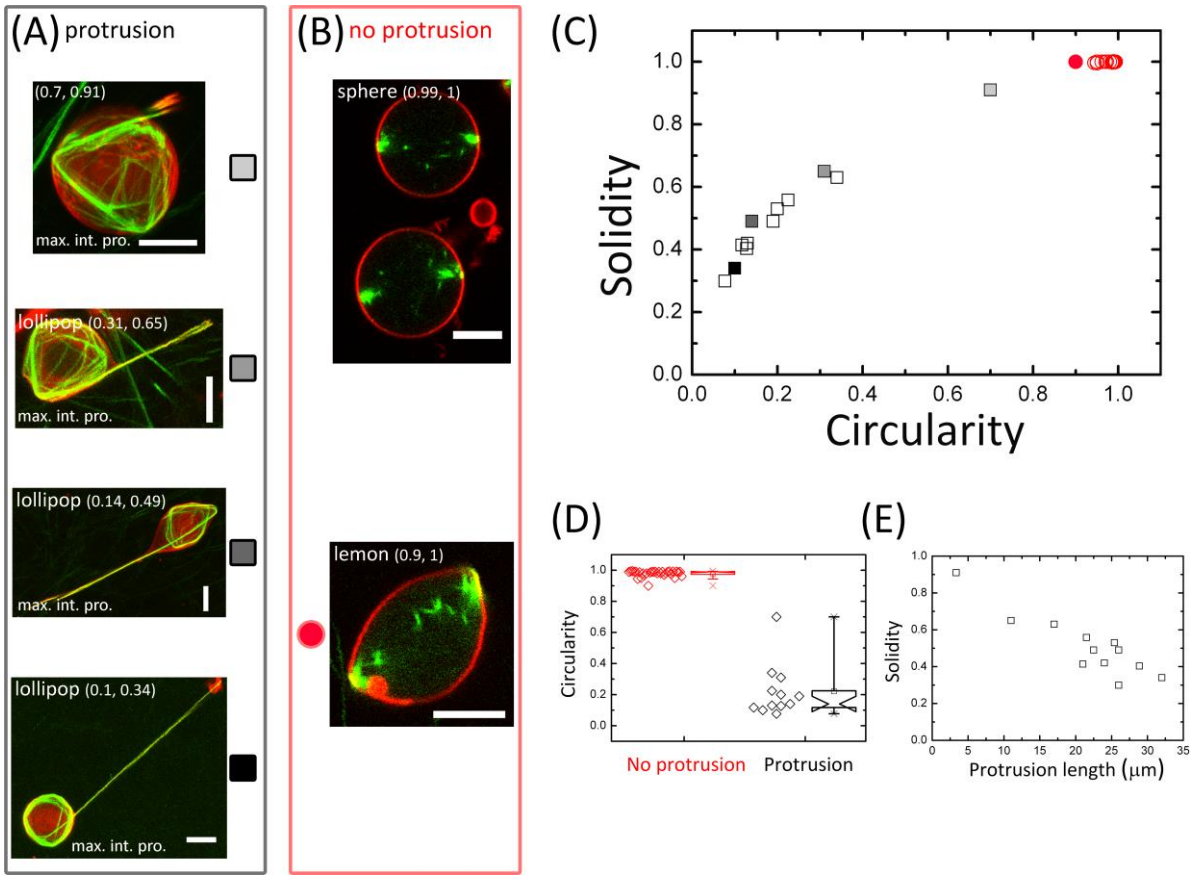

FIGURE S7 Morphological characterization of a population of 43 liposomes encapsulating actin-fascin bundles (R_F = 0.05) at the *stiff membrane* condition, where neutravidin molecules are bound to the liposome membrane via biotinylated lipids. (*A* and *B*) Confocal images of liposomes that are increasingly deformed (*top* to *bottom*). In (*A*), maximum intensity projections (*max. int. pro.*) of confocal sections of liposomes are shown where the number of planes (p) over a total z-range (z, in μm) are (p = 30, z = 14.5), (p = 17, z = 8), (p = 19, z = 9), (p = 24, z = 11.5) from *top* to *bottom*. In (*B*), images are confocal sections recorded at the equatorial plane of the liposomes. Red: membrane, green: actin. Scale bars: 5 μm. (*C*) Liposome shapes are summarized in terms of circularity and solidity. Reddish symbols represent liposomes having no protrusion (31 liposomes) and black/grayish symbols represent liposomes with one protrusion (12 liposomes). Color-coded solid symbols correspond to images of liposomes in (*A*) and (*B*). (*D*) Circularities of liposomes with and without protrusions. (*E*) The solidity is inversely correlated with the protrusion length (correlation coefficient = -0.9057, $p < 0.001$).

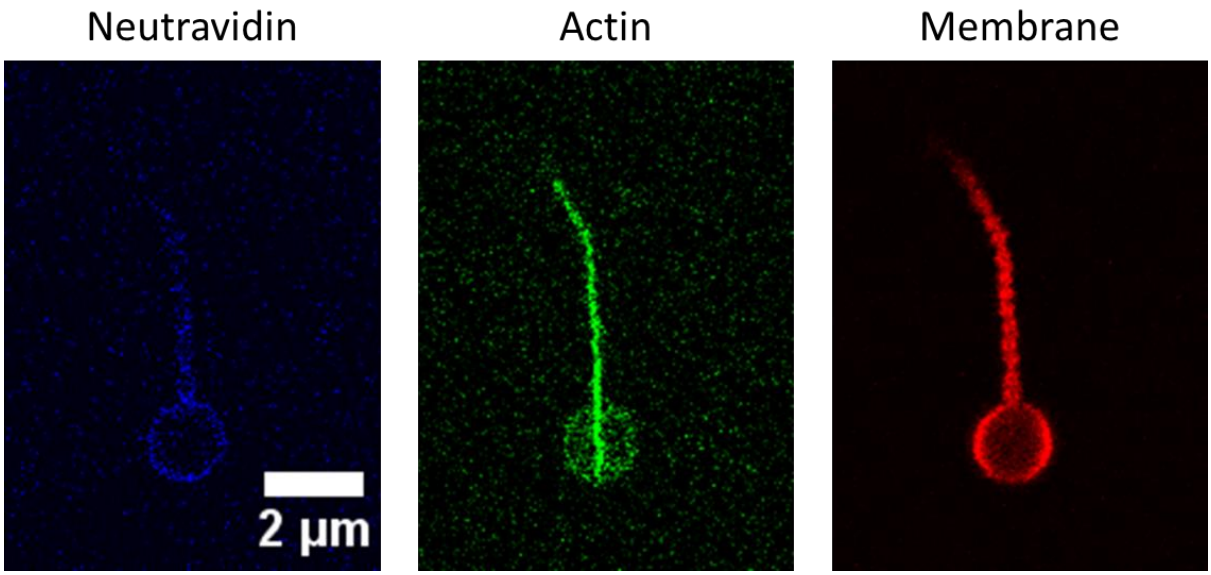

FIGURE S8 Liposomes encapsulating actin-fascin bundles formed at the *stiff membrane* condition, obtained by decorating the membrane with Alexa350-labelled neutravidin. The neutravidin signal (*left*) co-localizes with the membrane signal (*right*) along the liposome main body and protrusion.

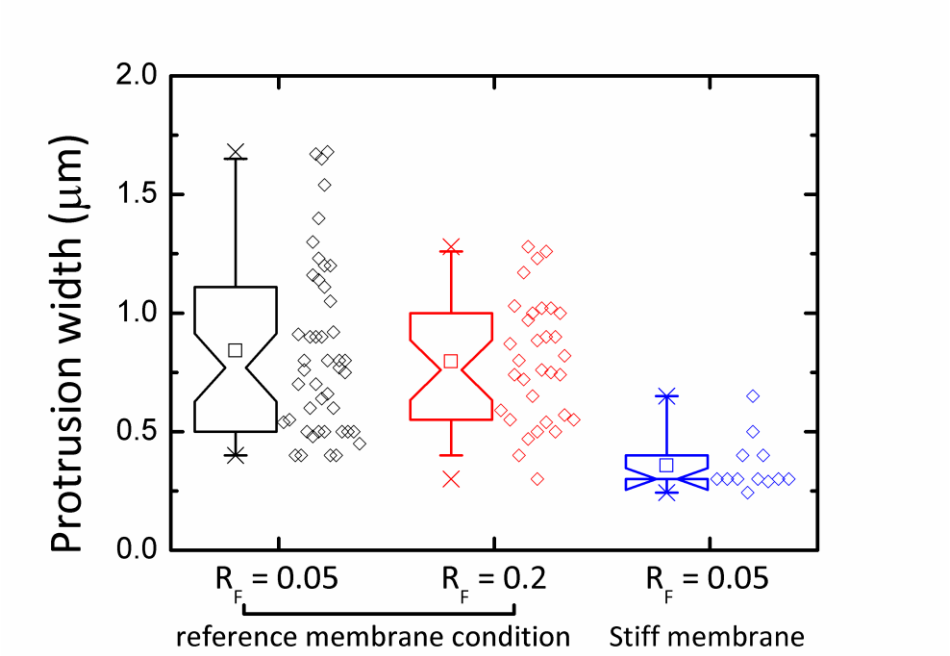

FIGURE S9 Influence of actin bundle stiffness (modulated by R_F) and membrane stiffness (modulated by decorating the membrane with neutravidin) on liposome protrusion width. Liposome population sizes from left to right: 45, 32 and 12.

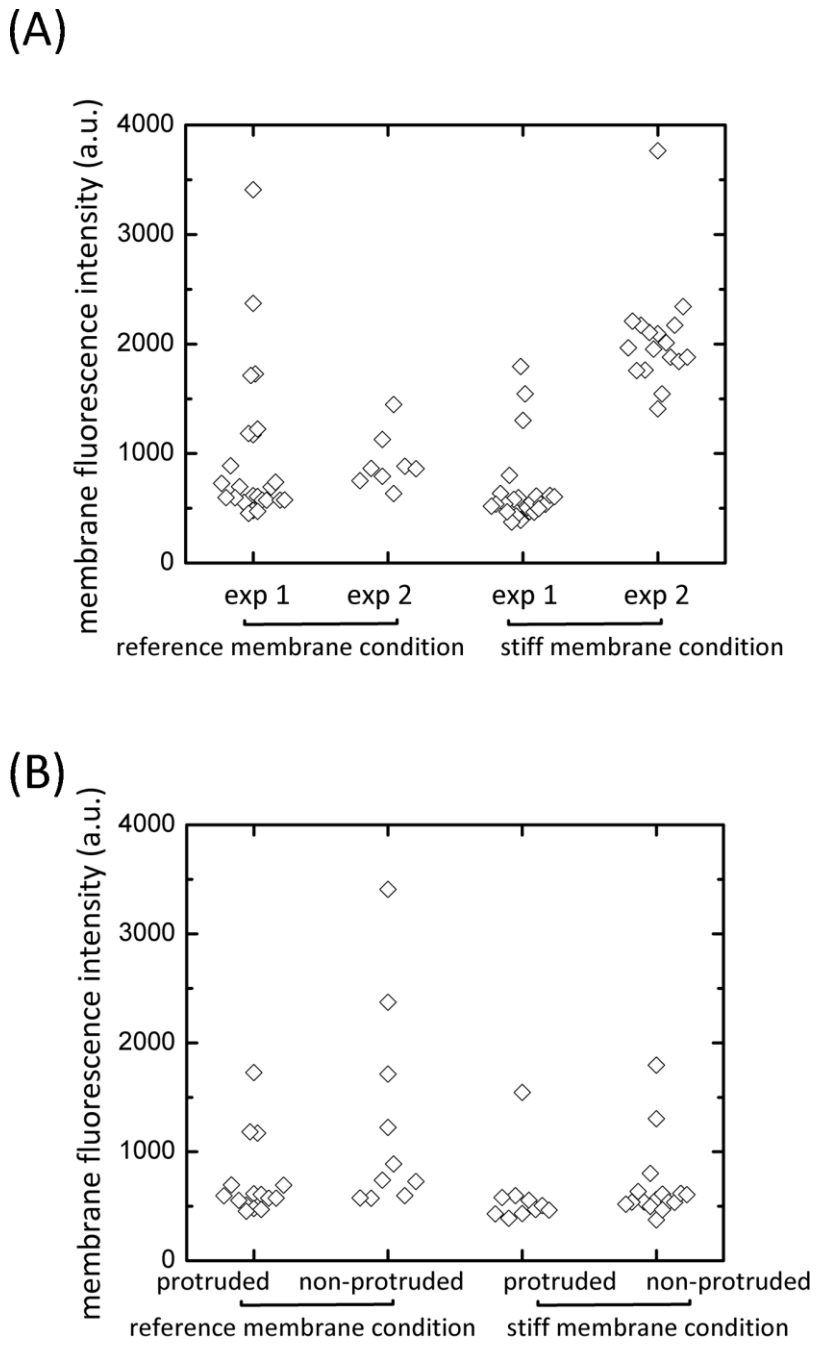

FIGURE S10 Test of membrane lamellarity distribution. (A) Membrane fluorescence intensities of liposomes at the *reference membrane* condition and at the *stiff membrane* condition. We note that the membrane image corresponding to the data point that has the highest membrane fluorescence intensity value in *exp2* at the *stiff membrane* condition has a few pixels having fluorescence intensity values exceeding the pixel bit depth. Liposome population sizes from *left* to *right*: 25, 8, 26, 17. (B) Membrane fluorescence intensities of liposomes with and without protrusions obtained in *exp1* at the *reference membrane* condition and at the *stiff membrane* condition. Liposome population sizes from *left* to *right*: 15, 10, 10, 16. There is no correlation between membrane fluorescence intensity (i.e. lamellarity) and the likelihood of membrane protrusions.

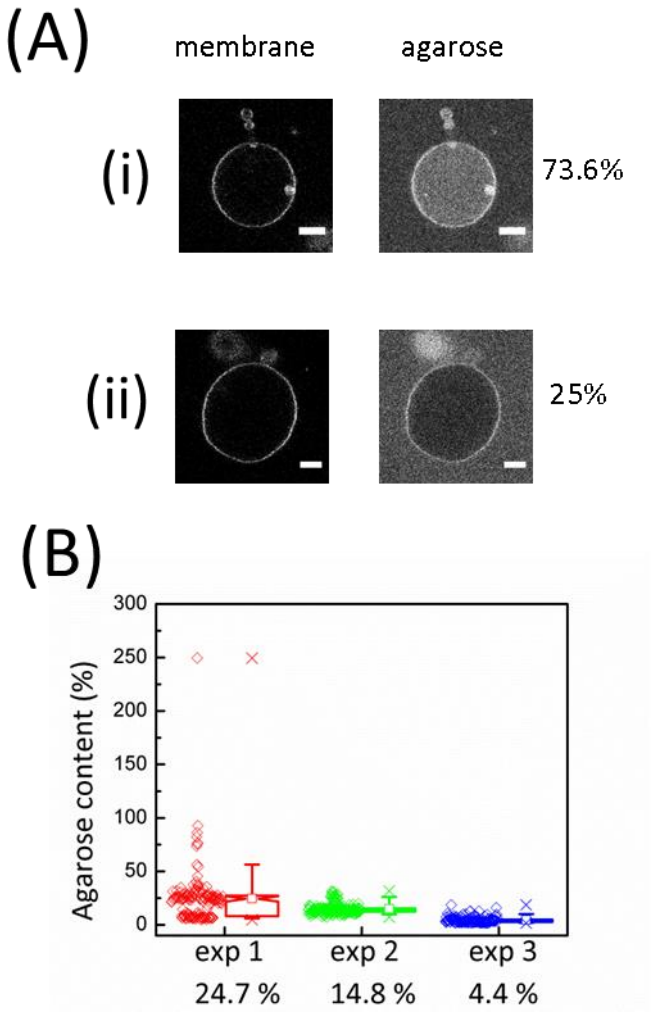

FIGURE S11 Agarose content in liposomes, quantified by the fraction of a 1% (w/w) agarose solution that remains inside the liposomes after formation. (*A*) Confocal fluorescence images of two liposomes, (*i*) and (*ii*). *Left*: fluorescence signals of liposome membranes. *Right*: fluorescence signals of fluorescently labelled agarose. (*B*) Agarose content in liposomes with population sizes from left to right: 145, 187 and 156. The average value of agarose content in each experiment is indicated below the graph. Note that in one liposome the agarose content is 250%, indicating a high concentration of agarose inside the liposome, perhaps due to a crowding phenomenon.

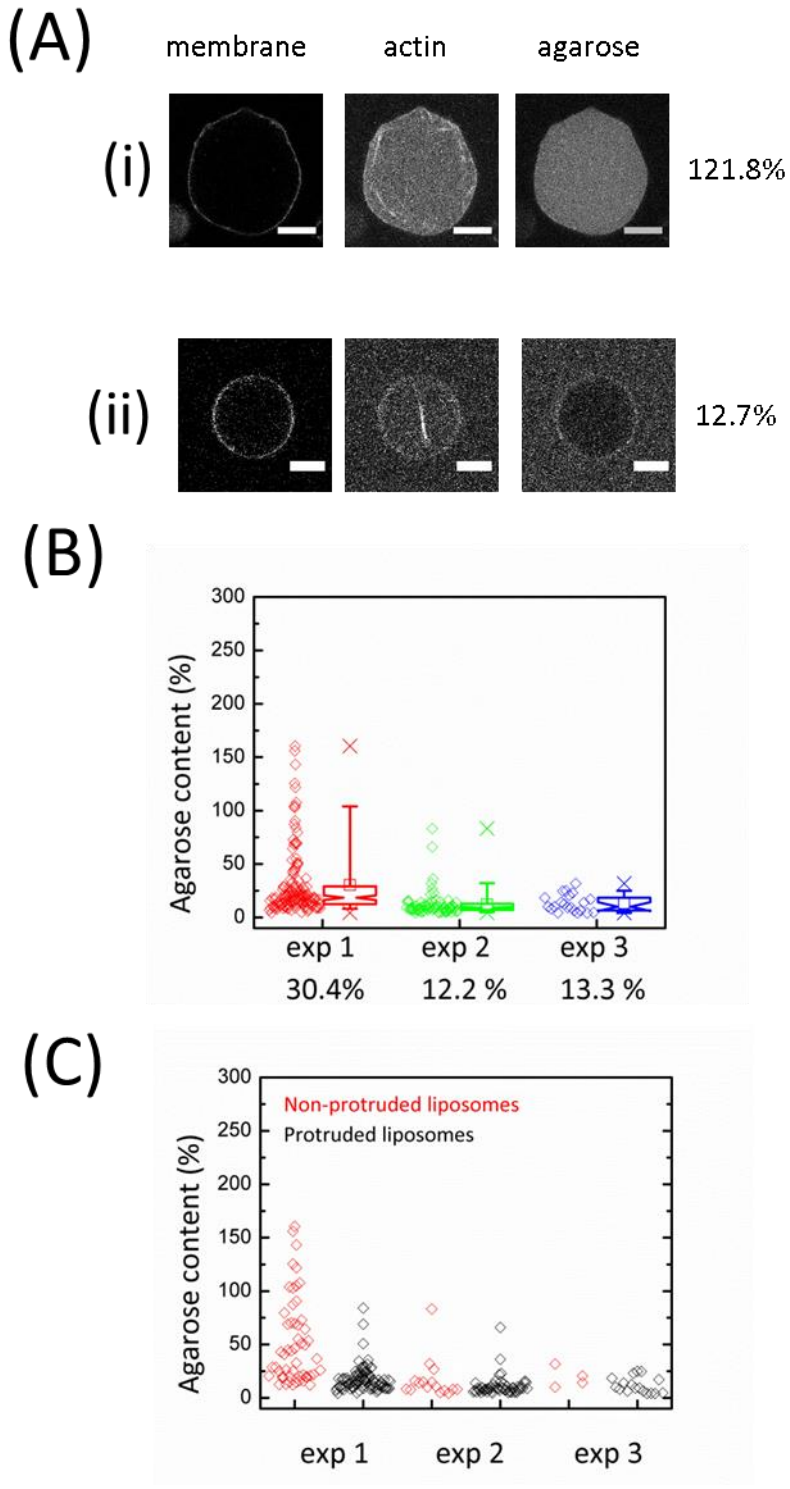

FIGURE S12 Agarose content in liposomes encapsulating actin-fascin bundles, quantified by the fraction of a 1% (w/w) agarose solution that remains inside the liposomes after formation. (*A*) Confocal fluorescence images of two liposomes, (*i*) and (*ii*), and their corresponding agarose content. In (*B*), the average value of agarose content in each experiment is indicated below the graph. In (*C*), for each experiment, the agarose content of liposomes with and without protrusions is shown separately. Liposome population sizes from left to right: (B) 143, 72 and 21, (C) 53, 90, 16, 56, 4 and 17.

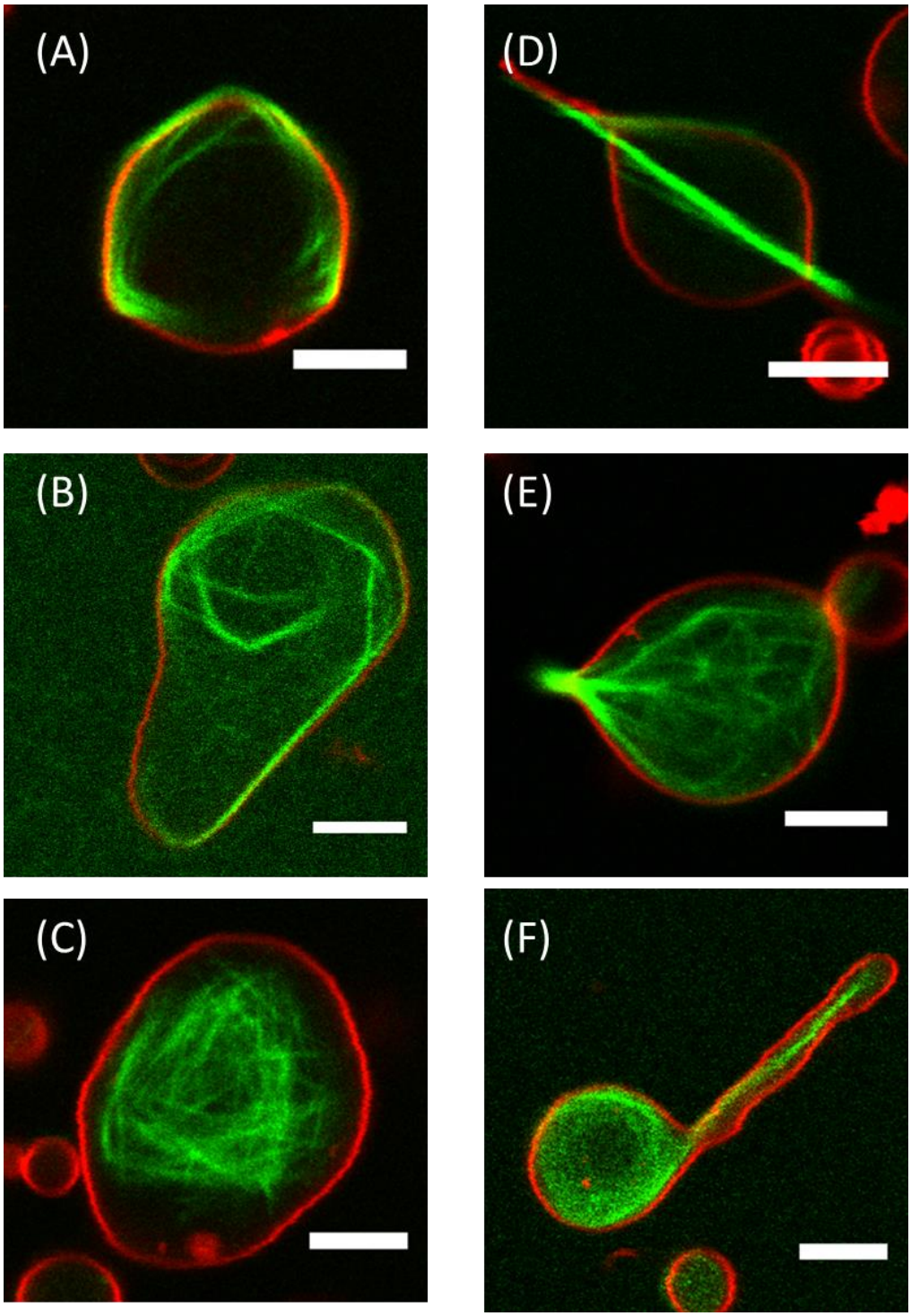

FIGURE S13 Confocal fluorescence images of PVA-formed liposomes encapsulating actin-fascin bundles (R_F = 0.05). Similar to agarose-formed liposomes, we observe a range of morphologies, from non-protruded, to lemon-like, and protruded. Red: membrane, green: actin. Scale bars: 5 μm.

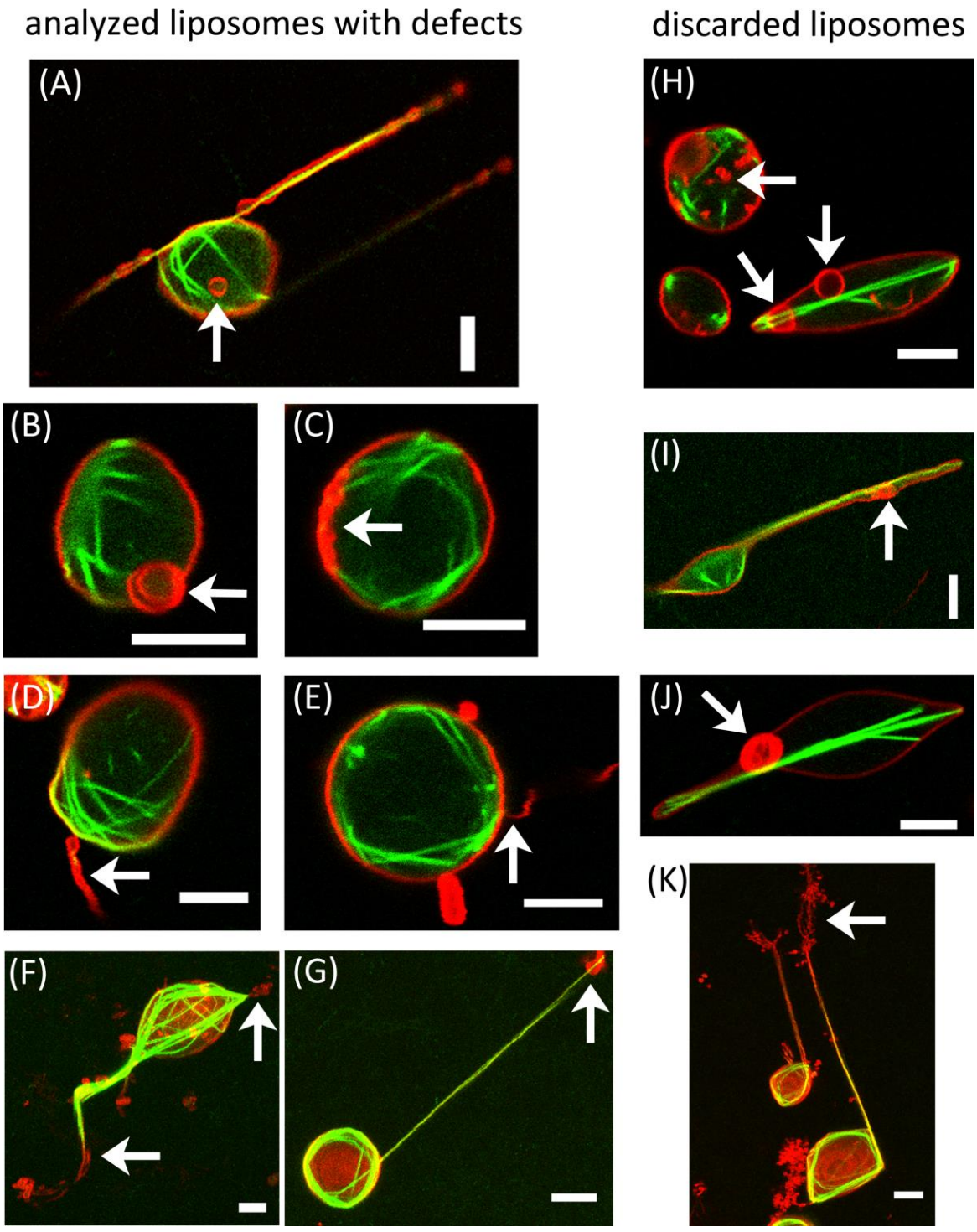

FIGURE S14 (*A*-*G*) Confocal fluorescence images of liposomes having defects that are deemed sufficiently minor to include in the morphological analysis (around 5% of a total of 70 liposomes at the *reference membrane* condition). Defects included: (*A*) a smaller liposome inside a larger liposome, (*B* and *C*) smaller liposomes adhered to the inside of liposome main bodies, (*D* and *E*) membrane tubes adhered to liposome membranes, and (*F* and *G*) membrane aggregations or tubes adhered to the end of a protrusion or to the main body of liposomes. (*H*-*K*) Confocal fluorescence images of liposomes that are discarded from the analysis because membrane shape and/or actin organization are potentially affected by the encapsulated membrane tubes or aggregates, as indicated by the white arrows (around 30% of a total of 70 liposomes at the *reference membrane* condition). Images are single confocal

sections recorded at the equatorial plane of the liposomes, except for (*F*), (*G*) and (*K*), where maximum intensity projections are assembled from 31 planes over a total z-range of 15 μm in (*F*), 24 planes over a total z-range of 11.5 μm in (*G*) and 20 planes over a total z-range of 9.5 μm in (*K*). Red: membrane, green: actin. Scale bars: 5 μm.